The Thesis Committee for Brendan Michael Elliott
Certifies that this is the approved version of the following Thesis:

Development of a New Analytical Model to Interpret Inter-well Poroelastic Pressure Transient Data

APPROVED BY
SUPERVISING COMMITTEE:

Mukul Sharma, Supervisor

John T. Foster

Development of a New Analytical Model to Interpret Inter-well Poroelastic Pressure Transient Data

by

Brendan Michael Elliott

Thesis

Presented to the Faculty of the Graduate School of

The University of Texas at Austin

in Partial Fulfillment

of the Requirements

for the Degree of

Master of Science in Engineering

The University of Texas at Austin

May 2020

Dedication

The entirety of this work is dedicated to my beautiful wife, who has uprooted her life to join me in this quest in Austin. I couldn't have done this without her love, support and editing skills.

I also would like to thank all the friends at UT who have helped me along the way and provided fruitful comments and brainstorming sessions. I have never been in a room of smarter, more intelligent individuals than the research lab.

And finally, Dr. Sharma who has provided the guidance, and insight to chase down and run with ideas. His unique leadership style allows for truly exceptional concepts to germinate and flourish.

Acknowledgements

I would like to acknowledge the vast body of work the industry has shared and published on the topic of well interference. We are truly standing on the shoulders of giants.

I would especially like to acknowledge the contributions of Dr. Ripu Manchanda, who has guided me through this workflow and provided exceptional insights and friendship.

Abstract

Development of a New Analytical Model to Interpret Inter-well Poroelastic Pressure Transient Data

Brendan Michael Elliott, M.S.E.

The University of Texas at Austin, 2020

Supervisor: Mukul Sharma

Pressure interference data between fractured wells in unconventional formations during fracturing has been shown to yield great insights into the geometry of propagating fractures. Interpretation of this pressure response data can be used to estimate key unknown fracture parameters such as azimuth, height, width, and length. This pressure interference is ascribed to the poroelastic impact of the propagating fracture's stress shadow. Numerical modeling of these measurements using fully coupled geomechanical simulators has been shown to history match field observations. Numerical modeling, however, can be time-consuming and not feasible for application in on-the-fly solutions during the frac treatment. There is a need for simple, high-speed tools that can guide the staff and engineers on location with insight into the position and geometry of the propagating fractures. This work presents a new analytical model that provides a method for quick analysis of the fracture responses from downhole pressure gauges during treatment, validation with fully 3-D coupled numerical modeling, and successful application to field cases.

This new analytical model uses the fundamental stress equations for simple fracture geometries (KGD, PKN, and radial fractures) and captures critical characteristics observed in field pressure interference observations. Multiple field stages with offset pressure responses were captured with bottom-hole gauges, interpreted, and detailed in this body of

work. A Python code for these analytical stress predictions was developed to make the process user-friendly and adaptable to ever-changing industry needs.

The model closely ties these observed field responses to predicted stresses reported from the model and allows for timely interpretation of the pressure data. To further validate the characteristic stress responses observed in the field, fully coupled 3-D poroelastic simulations were also performed with results showing less than 2% error relative to the analytical predictions. Insights into well spacing, fracture geometry, fracture overlap, and stress shadow with varying distances are obtained from the results.

This workflow can be employed for near real-time analysis and yield estimates of fracture geometry to greatly advance the field capabilities for on-the-fly fracture design optimization.

In an industry with increasing complexity in nearly every model, this work shows that simple ground truth physics and analytical results can be extremely useful tools to make quick, effective decisions with minimal computational resources.

Contents

List of Figures

List of Tables

Chapter 1. Introduction[1]

As multi-well pad operations become more complex and the natural variability of the formations is better recognized there is a continual need to advance tools utilized for fracture characterization. Pressure interference between wells in low permeability systems is induced by poroelastic interactions (not by pressure diffusion) during fracturing. This has been well documented in recent literature and has been used to estimate fracture parameters such as azimuth, length, width, and height of the fracture (Kampfer et al. 2016; Roussel and Agrawal 2017) There have been extensive numerical modeling of this poroelastic phenomenon using fully coupled geomechanical simulators (Seth et al. 2018, Seth et al. 2019). These results have been compared to field observations and confirmed with diagnostics (Daneshy et al. 2012, Dawson et al. 2016, Spicer et al. 2019). However, numerical modeling of this process is time consuming and does not lend itself to a near real-time, or real-time explanation of offset pressure signals. It is almost always done after the fracturing treatment is complete as a matching exercise with field data. The efforts in this work show a new, analytical model workflow that will better fit the expectations of speed and accuracy that modern unconventional completions require.

The poroelastic pressure changes of concern for this application require a coupling between the stress interference induced by a propagating fracture and the pore pressure in the reservoir. Numerical modeling is useful for characterizing the stress interference induced by arbitrarily shaped fractures, however some simpler geometries can be represented using analytical solutions.

Sneddon (1946) described the distribution of stress around a pressurized line crack and provided formulae to evaluate the components of stress at any point in the 2-D medium. Their solution assumes that width does not vary in the vertical direction, and a state of plane strain exists

1 Many ideas and concepts presented in this thesis have been sampled from previously published works from the author. Contributions from this author include early development of the analytical model, validating with numerical simulations, and implementation and validation with actual measured field data.
Elliott, B., Manchanda, R., Seth, P., & Sharma, M. (2019, July 31). Interpreting Inter-Well Poroelastic Pressure Transient Data: An Analytical Approach Validated with Field Case Studies. Unconventional Resources Technology Conference. doi:10.15530/urtec-2019-449.
Manchanda, R., B. Elliott, and M. M. Sharma, "Interpreting Inter-Well Poroelastic Pressure Transient Data: An Analytical Approach", 53rd US Rock Mechanics / Geomechanics Symposium, New York, New York, U.S.A., June 23-26, 2019, American Rock Mechanics Association, 06/2019.

in the horizontal layer. The same work provides descriptions for a 3-D model but is limited to a "penny shaped" geometry, not widely accepted as applicable to unconventional stimulations. Green and Sneddon (1950) describe the formulation of an elliptical crack that is opened by a constant pressure along the face of the crack. Their solution is rather elaborate and obtaining a general solution of the stresses induced in the 3-D space surrounding the crack is difficult.

Warpinski, Wolhart, and Wright (2004) provide a summary of the methods required to calculate the stresses induced by an elliptical crack and capture the stress interference along the horizontal plane passing through the center of the vertical elliptical crack. This work provides a solution to estimate stress and pressure away from a fracture in any vertical plane, while also capturing the pressure degradation down the fracture that allows for variable width along all portions. There is little evidence of any prior work that can utilize results that capture the stress changes in the reservoir in a horizontal plane away from a fracture with finite height.

Daneshy (2014) provides a detailed review of the 2-D elliptical stress shadow model with its application to field data, which includes intra-well and inter-well shadowing using the estimates of stress derived from the 2-D analytical method for wells in the same horizontal landing. Daneshy (2017) cites several reasons why field data may not agree with calculations done using a 2-D model including stiffness reductions from previous fractures, gradual closure, variable net pressure, and deflection paths.

This work presents a new model that uses the learnings from the 2-D model and extends it to overcoming the shortcomings of earlier models. This new model has been developed for finite height fractures and can calculate the stress changes induced above/below and normal to the fracture in 3-D space. This calculation of stresses induced by a PKN type fracture (i.e. no constant pressure assumed inside the fracture) has not been done before.

Field data has shown evidence of the pressure changes in a monitoring well induced by the propagation of a hydraulic fracture in its vicinity. This observed pressure change is caused by the poroelastic impact of the induced stress interference. An analysis of the different factors affecting

these pressure changes is provided. Additionally, an investigation is made to suggest methods to interpret the pressure changes observed in the field by using the newly developed model.

Chapter 2. Thesis or Project Statement

In the last decade unconventional development has exploded and matured, well developments have gone from single wells per section, to closely stacked, staggered full unit developments. New tools are needed to quickly diagnose, understand and react to field observations of pressure responses during fracturing. This Thesis seeks to develop analytical tools to build the foundation of real time interpretation of fracturing pressure signals, and validate such models with known numerical solutions, and field case studies.

Chapter 3. Existing Literature and Significant Prior Research

This section will review recent literature on fracture driven communication and poroelastic pressure responses, their causes, and effects, and it will investigate learnings that the industry has derived from interpreting these signals. The background research will review current work and is not meant to be an exhaustive list, but rather, a concise description of contemporary industry understanding and technical capability.

A conceptual model is introduced (Figure 1) to set the framework of the issue at hand. Barree et al. (2017) presents an illustration of modern unconventional developments. A large drainage pattern for standalone parent wells is established, with the dashed red lines representing induced hydraulic half lengths of the fractures. There are smaller effective producing lengths, but in general, the parent wells drain the reservoir unbounded on either size. Upon infill development, the child wells are typically drilled within this initial fractured region of the parent well or very close to it. The parent well depletion causes a pressure and stress reduction in the reservoir and induces fracture asymmetry when the child well is completed. This asymmetry in child well geometry and lower pressures in the reservoir cause underperformance, and the fracture driven communication from the child well's stimulation can damage the parent well, causing loss of produced reserves. Fracture driven communication (FDC) can be known by many names: "Frac Hits," "Bashing," "parent-child interference," fracture shadowing, or poro-elastic signals, but this section will be diligent and consistent in citing authors' naming conventions and attempt to distinguish the nuances between each.

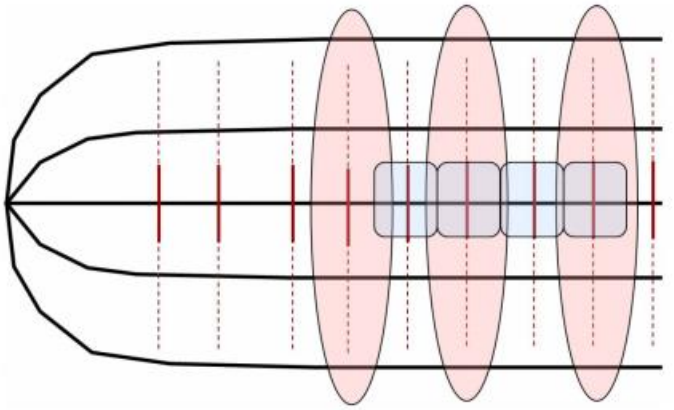

Drainage pattern established by pattern drilling of horizontal wells. The black lines represent the horizontal well sections, the red dashed lines the hydraulic half-lengths present while pumping a treatment (and can lead to "bashing"), and the solid red lines represent the effective production length.

Figure 1: Conceptual model for horizontal well development

It is important to note there are two main categories of FDC that can be distinguished with simple pressure observations: 1) a direct fracture hit or fracture intersection with the subsurface monitor and 2) an elastic signal of a fracture passing nearby an existing fracture or monitor fracture. Below in Figure 2**,** obvious differences between the two cases are shown. Fracture hits generally increase parent well pressure by multiple hundreds of pounds per square inch in a very short timeframe (minutes), while elastic signals (circled) can be single digit to a few hundred pounds per square inch and occur over a much larger time frame (tens of minutes to hours, depending on length of pump time).

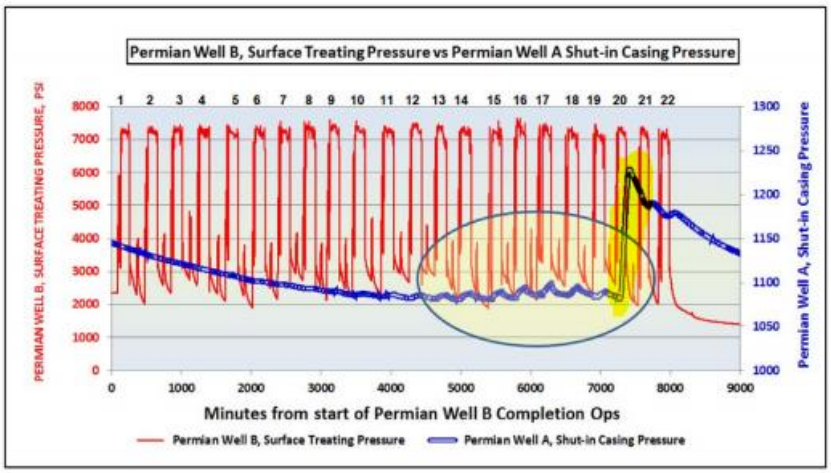

Figure 2: Case Study example of fracture shadow (elastic responses) transitioning to frac hits (fracture to fracture intersection) From SPE 189853

Published cases of fracture hits, fracture driven communication, and parent child relationships did not become numerous until the last few years, as these are new topics that operators are experiencing in the later stages of field development and infill drilling. Most of the recent literature can be broken up into four main categories: dynamic pressure analysis, production or well interference analysis, advances in modeling, and field case studies. Dynamic analysis, numerical modeling, and field cases will be explored here.

Figure 3 shows the results from a OnePetro keyword search of "Parent," "Child," and "Frac Hit(s)." A sharp increase in published cases for these topics occurred in 2014. This increase in literature (at an astounding rate from less than 5 papers per year to 45+ papers per year estimated for 2018) indicates the early recognition from technical staff and academia of the significance of the issue. The image on the right is derived from quarterly calls with public companies, and investor relations decks where management mentions the related topics of "parent-child" and "frac hits." Again, we see a sharp increase and inflection point but this time slightly later in time (2016-2017). This can likely be described as a learning curve or perhaps a comfort level of management discussing these issues publicly.

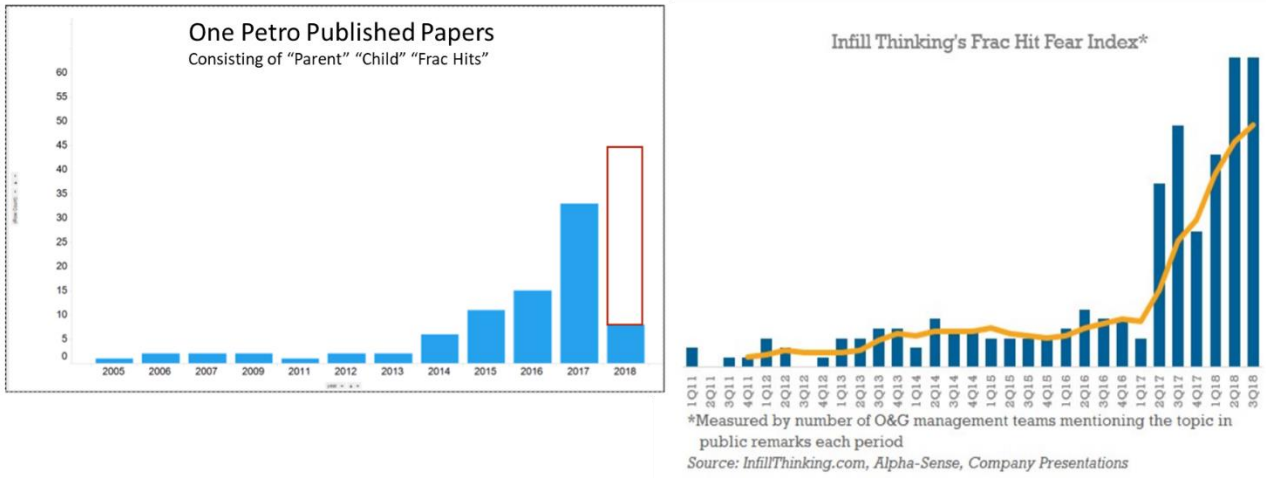

Figure 3: Left: Data pull of published literature with titles consisting of key words. (Right): infill thinking diagram for investor relation reports where management mentions topics of frac hits or parent child (from HFTC Plenary Session Presentation Elliott, 2019)

Another interesting relationship can be seen in Figure 4**.** It wasn't until 50% of the new wells drilled were child wells that the issue became significant enough for the "technical paper" inflection to happen, before this point, very few wells were drilled together, and the industry was in a leasehold preservation phase, developing many single well sections with little to no chance of observing well to well communication. These examples show the recent interest and importance of fracture interference and exemplify the timeliness and relevance of the research and review of potentially unresolved issues.

Figure 4: Percentage of new parent wells drilled vs child wells in the Eagleford (modified from SPE 189875)

3.1 2-D STRESS SHADOW

The fundamental line crack model discussed in Sneddon (1946) assumes plane strain in the height direction. This model calculates the incremental stress induced in the plane of the propagating crack with a uniform net pressure opening the crack. Using this model, the volumetric stress change induced by a fracture can be calculated at any location in the plane of the fracture using Eq. (1). The coordinate system used is described in Figure 5 and the model schematic is shown in Figure 6.

$$\Delta\sigma_V = P_{net}\left[1 - \frac{r}{\sqrt{r_1 r_2}} cos\left(\theta - \frac{\theta_1 + \theta_2}{2}\right)\right] \quad (1)$$

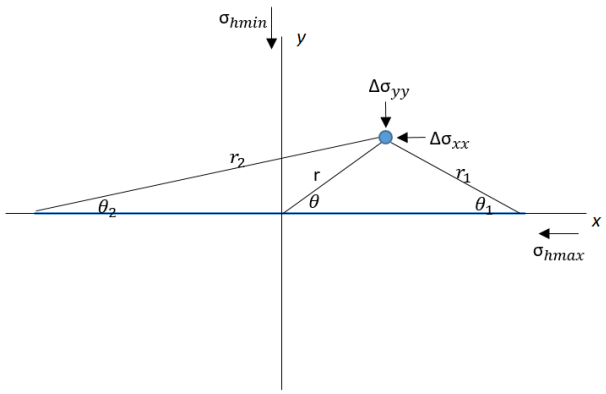

Figure 5: Coordinate system around a 2-D plane strain fracture.

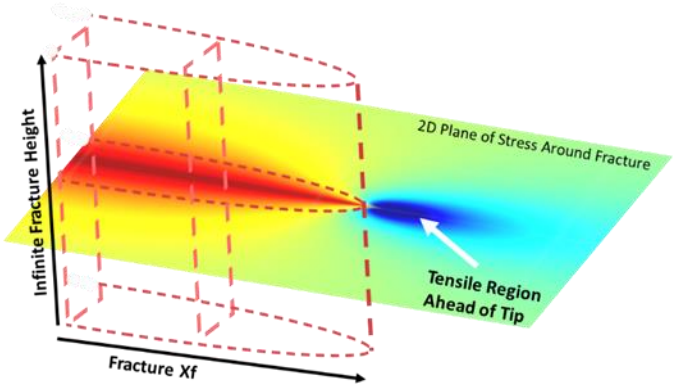

Figure 6: Representation of an infinite height 2-D fracture with resulting stresses contours in a horizontal slice.

3.2 DYNAMIC ANALYSIS OF PRESSURE DATA

The dynamic pressure analysis includes the evaluation of the active well stimulation and direct fracture driven communication on offset wells, or "Frac Hits." These are often seen as detrimental to the parent wells and caused by various issues**.** There is also a rather large group of literature evaluating the poroelastic nature of the stress shadow on offset wells and monitor fractures. These techniques have been developed to identify fracture geometry and evaluate completion designs.

Daneshy, (2012) reviews many topics on intra-well and inter-well communication and performs a general analysis on field pressure data, through which he is able to determine fracture

orientation, initiation pattern, fracture height, communication character, extension, fluid exchanges, and post-frac communication. He cites this project as the first discovery of the "fracture shadowing" theory and techniques. Later, in a 2014 paper, Daneshy gives the background, theory, and applications for this fracture shadow concept. Citing the original 2-D Sneddon solution from 1946, Daneshy describes the model interpretation for stresses induced by an active extending fracture (Figure 7).

$$\sigma_y + \sigma_x = 2\Delta P \left\{ \frac{r}{(r_1 r_2)^{1/2}} \cos\left(\theta - 0.5(\theta 1 + \theta 2)\right) - 1 \right\}$$

$$\sigma_y - \sigma_x = 2\,\Delta P\, \frac{r\,sin\theta}{X_f} \left(\frac{{X_f}^2}{r_1 r_2}\right)^{\frac{3}{2}} sin\frac{3}{2}\,(\theta_1 + \theta_2)$$

$$\tau_{xy} = \Delta P\, \frac{r\,sin\theta}{X_f} \left(\frac{{X_f}^2}{r_1 r_2}\right)^{\frac{3}{2}} \cos\frac{3}{2}\,(\theta_1 + \theta_2)$$

Figure 7: 2-D Sneddon solution for stress distribution in the neighborhood of a crack.

These concepts were used to form the basis for the various methods of interpretation shown below in Figure 8**.** These surface pressure responses are clearly known now as to be poroelastic responses from the actively fracturing well and have since been measured on thousands of stages pumped by multiple operators. It should be noted that these responses are very different from "frac hits," which are characterized as direct fluid communication to the observation wellbore with large pressure spikes of greater than hundreds of pounds per square inch, while a shadow response or elastic response can manifest in tens of pounds per square inch and occur over a longer duration of five to ten minutes.

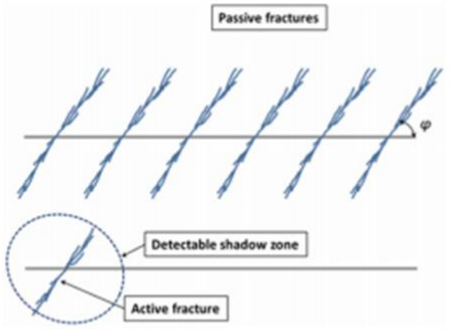

Figure 8—Schematic of fracture shadowing in offset wells

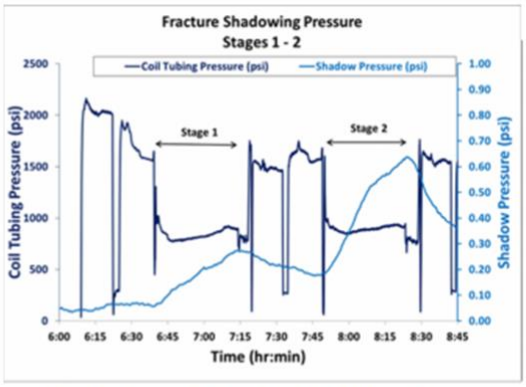

Figure 9—Fracture shadowing in offset wells (case history)

Figure 8: Fracture Shadowing Schematic and pressure Response from Daneshy SPE 170611

Lehmann et. al. (2016) presented an excellent paper on the dynamic analysis of frac hits and inter-well connectivity in the Horn River Basin. They very elegantly describe the response characteristic of the pressure hits into four main components in Figure 9. First is the time delay, or difference observed between the start time of an offsetting hydraulic fracture stimulation and the observation of a pressure response; the value is interpreted as the distance covered by the fracture or as proof for the existence of connections between wells. The intensity, or rate of pressure increase observed in the passive wellbore, is the second component and presents information on conductivity or connection between wellbores. Thirdly, the magnitude, or peak pressure observed in the passive well, captures active stimulation pressure and yields a degree of connectivity. The final component, falloff, or the rate of unsupported pressure decline observed after cessation of an active stimulation, gives insight into network complexity and system leakoff.

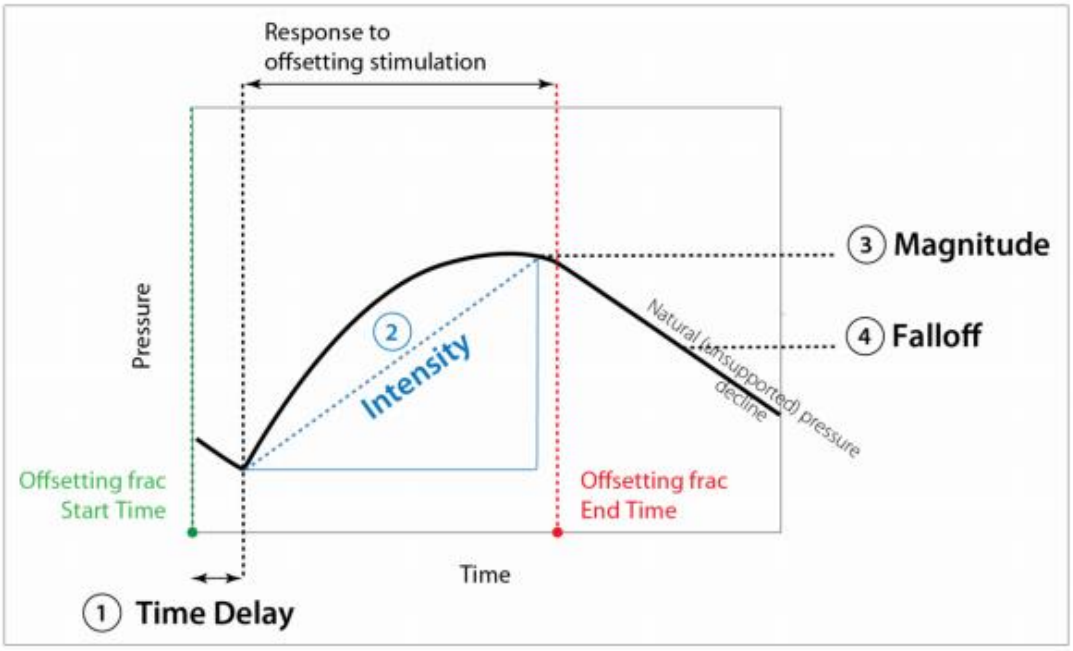

Figure 9: Pressure Hit Characterization from SPE 179173

Litchfield & Lehmann, (2013) describe inter-well communication through the fractures and show that flow connections may be frequent and time sensitive. Figure 10 indicates short term and long term connections indicating the fracture driven, well connections are temporal in nature and generally close during sustained production.

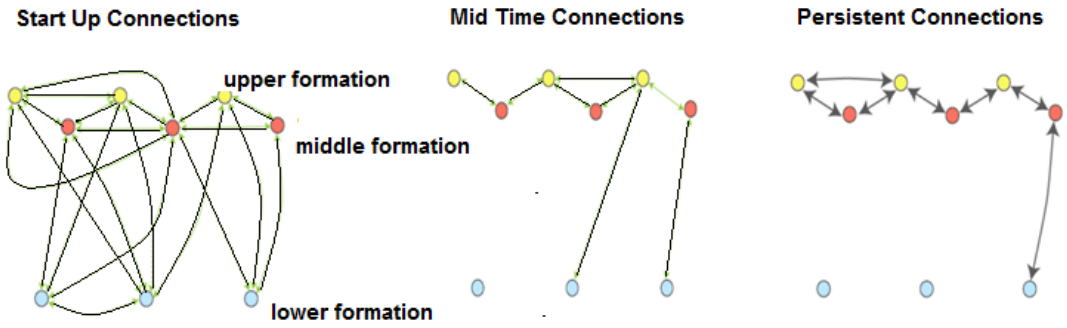

Figure 10: Well Communication example through time from Litchfield & Lehmann (2013)

Roussel & Agrawal (2017) give an introduction to poro-elastic response monitoring and quantify fracture geometry from offset pressure monitoring. The method described uses the poro-

elastic pressure responses on offset treatment wells and provides a solid framework for the theory and use of fracture signals. The paper includes support from modeling and justification from numerical simulations (Figure 11), which show the elastic response of the offset fracture growth. This paper also discusses critical differences between direct frac hits and poro-elastic responses.

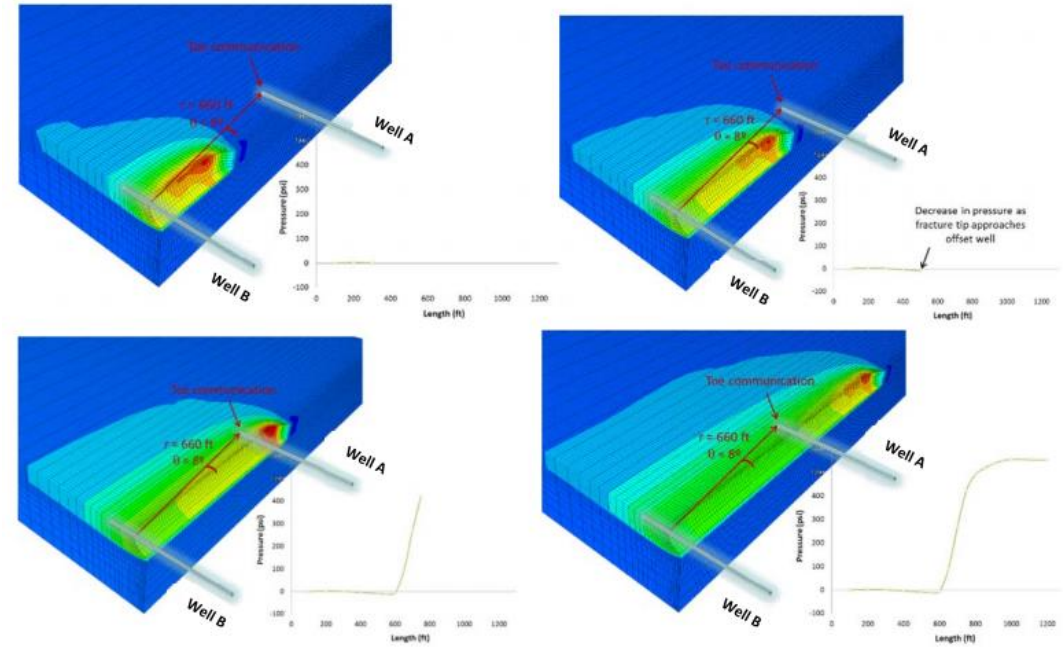

Figure 11: Evolution of poro-elastic response measured in offset well A during propagation of stage 1 in well B From SPE 2645414

Seth et. al. (2018) further explain the work from Roussel and presents examples from their fully coupled 3D geomechanical poroelastic model that simulates the dynamic elastic signals observed in the field. They were able to successfully match the tensile region, response time, and overlap period that induces the response on monitor fractures. This allows for estimates of hydraulic fracture geometry to be made, as can be seen in Figure 12.

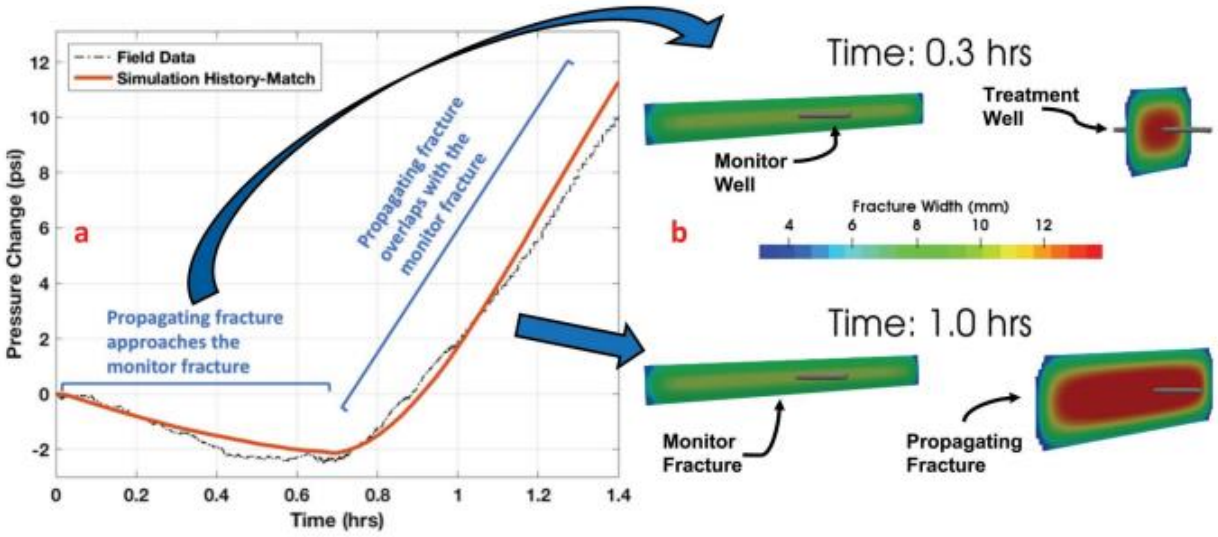

Figure 12: History Match of pressure change observed during fracture propagation in treatment well, with the 3d configuration of fractures. From SPE 191492

A service company is also offering this type of interpretation as a service. Spicer and Coenen (2018) describe the methods used, which expand upon the initial work by Dawson and Kampfer. They utilize global matches of the final pressure responses to estimate the fracture geometry from previously modeled stress responses, and then present a final solution for fracture geometry and stimulation effectiveness.

3.3 NUMERICAL ANALYSIS OF PRESSURE RESPONSE DATA

Advanced modeling efforts in this space are fairly new, and in particular the technology in coupled poroelastic simulators is only a few years old at most. Many of the published examples attempt to match field observed behavior with the models to show that the connection between wells can be explained by direct hydraulic fractures.

Yu et al. (2017) developed a numerical, compositional model to simulate well interference. The simulations showed connecting hydraulic fractures play a more important role than natural fractures in declining BHP of shut in wells. Matrix permeability had a minor impact on well

productivity, since the connecting or intersecting “frac hits” were the main driver of lower child performance.

Morales et al. 2016 utilized the Schlumberger modeling suite to show that after refracturing parent wells, stress deflection and re-pressurization of originally depleted zones will reduce fracture hits from infill wells. Refracturing was able to increase stress from 5,500 psi to 7,500 psi in the depleted area. The model also showed that in a case with no parent well refracturing, there was an expected frac hit from the infill child well.

Manchanda et al. (2018) displayed a 3D reservoir scale poroelastic geomechanics software in Figure 13 to model depletion and calculate its impact on pressure, total stress, and effective stress. They stated the three main factors that influence interference between parent and child wells are reservoir depletion, total stress changes, and effective stress changes.

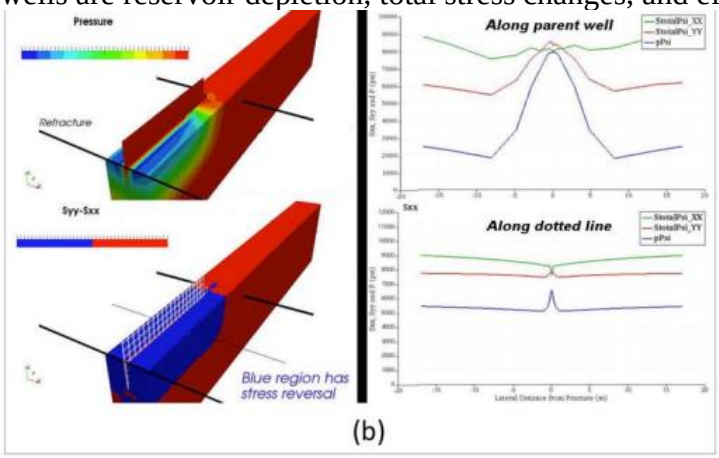

Figure 13: Impact of refracturing on the pressure and stress in the reservoir from Manchanda et al 2018.

Gala et al. (2018) developed a fully coupled compositional model to investigate fluid injection into depleted wells to minimize damage resulting from frac hits. He was able to simulate water and gas injection and the resulting effects on pressure and stresses in the reservoir.

Zhe et al. (2016) showed a model to describe the framework for bashed wells, modeling the mechanism, or fracture pressure interaction, and loss of fracture conductivity through time, and they history matched various cases during simulation.

3.4 INDUSTRY FIELD STUDIES AND QUANTIFICATION EFFORTS

In an extensively well cited paper by Miller et al. (2016), a multi-basin approach to identifying frac hits was introduced. Over 3,100 fracture interference events were evaluated in five basins. They defined seven parameters for positive and negative effects, then quantified which basins observe each respectively. These results are show in Figure 14. It is interesting to note the variability in each basin and the tendency for certain basins to observe negative effects, while others observe positive. This is noted as a major opportunity for research and potential future work to further identify why these variations are seen across basins.

	Bakken	Eagle Ford	Haynesville	Woodford	Niobrara
Positive Hit - Long Term	17%	9%	20%	2%	0%
Positive Hit - Short Term	33%	14%	38%	2%	6%
Positive Hit Total	**50%**	**24%**	**58%**	**4%**	**6%**
No Change	**35%**	**36%**	**24%**	**32%**	**38%**
Negative Hit Total	**15%**	**41%**	**19%**	**64%**	**56%**
Negative Hit - Short Term	7%	13%	5%	20%	19%
Negative Hit - Long Term	6%	17%	5%	41%	31%
Shut-in Post Offset Hit	2%	10%	9%	3%	6%
Instances Included	**649**	**1,210**	**366**	**259**	**32**
Original No. of Instances	827	1,561	449	283	49
Instances with Invalid Data	178	351	83	24	17

Figure 14: Quantification of positive and negative interferences by basin (Miller et. al. 2016)

In the same paper, several methods to prevent hits on parent wells were identified. Changing lateral landing zone, changing child well job design, re-pressurizing parent wells, refracturing parent wells, and utilizing chemical diverters were all explored.

Apache Corporation has been an outspoken player in the space with two major papers from King et al. (2017) and Rainbolt et al. (2018). These two papers characterized the framework for frac hit induced production losses in parent wells. They described the root causes, damage, and possible prevention methods. One of the key elements in these papers was the discussion of parent well monitoring and collecting data on fracture interference. They related magnitude of pressure changes to greatest production loss, showed little variation with landings and various benches to

the interference, and also investigated the slope of the responses, showing numerous examples of these well to well connections with surface level interpretation. It is important to note that most of the pressure responses in the paper were poro-elastic signals, rather than direct fracture communication.

Martinez et al. (2012) showed a case study with Exco Resources in the Haynesville wherein they described in detail the pressure sinks caused by parent well production and suggested a technique for mitigation in development programs. They primarily used designs (PSM1 & PSM2) that divert fracture energy away from the existing network, utilizing diverter and 100 mesh sand to contact new reservoir.

One of the earliest papers published on this topic was from Ajani et al. (2012), discussing the identification of the impact around infill wells. They attempted to quantify the impact using exponential decline to predict 60 day production rates and quantify a percentage of volume decrease in the impacted wells. One of the novel concepts presented was distance and age relationships that indicated wells 480 days old have a 40% chance of impact 1,000-2,000 ft away but a 72% chance of impact if less than 1000 ft away.

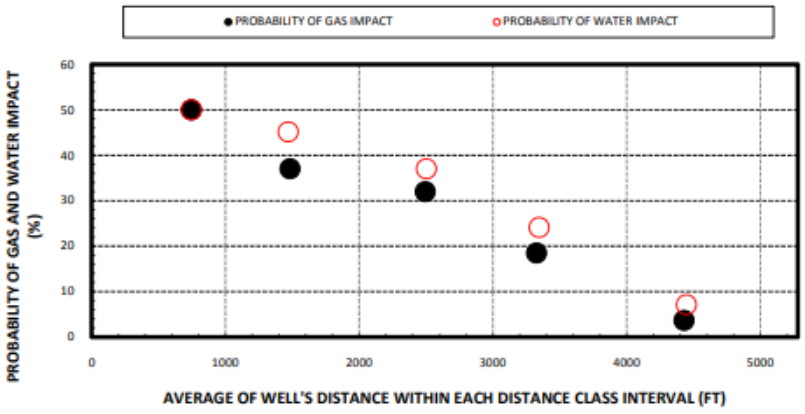

Figure 32: Probability of a Well Being Impacted Based on its Distance from Infill Well

Figure 15: Image from SPE 154045 showing probability of impact vs wells distance

The influence of treatment design, fluid type, pump rate, and perforation scheme on fracture interference has been published before. These publications show that varying completion style has a direct effect on the expected frac length, width, and height. Figure 16 below represents a three well case study in the Delaware Basin, (as described by Mack (2017)). Well 1H had been producing for approximately two years when the 2H and 3H were completed. The primary well (1H) was shut in and instrumented with bottom hole gauges, and surface and downhole microseismic arrays were installed throughout the location. The purpose of this study was to determine an optimum infill completion design and also understand fluid design's impact on the offset primary well response, with the intention of eliminating negative fracture interference events.

Design	Treating Fluids		Proppant Sizes	Stages
	Pad	Main		
A	Slickwater	Crosslinked Gel	20/40-mesh	1-3, 5, 6, 8-13, 15, 16, 18-22
B	Slickwater	Slickwater	100-mesh & 40/70-mesh	4, 7, 14, 17

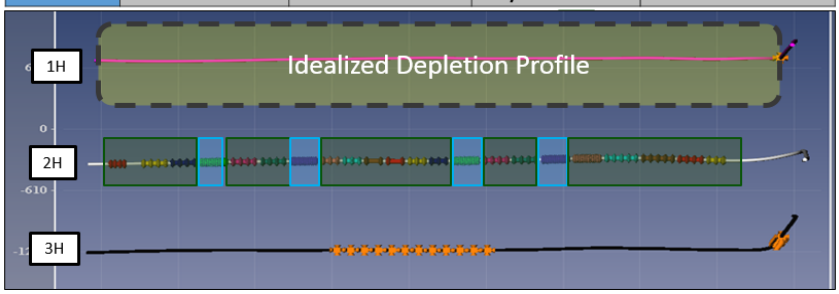

Figure 16: Figure of three well case study utilizing varying fluid systems to observe differences in hydraulic communication.

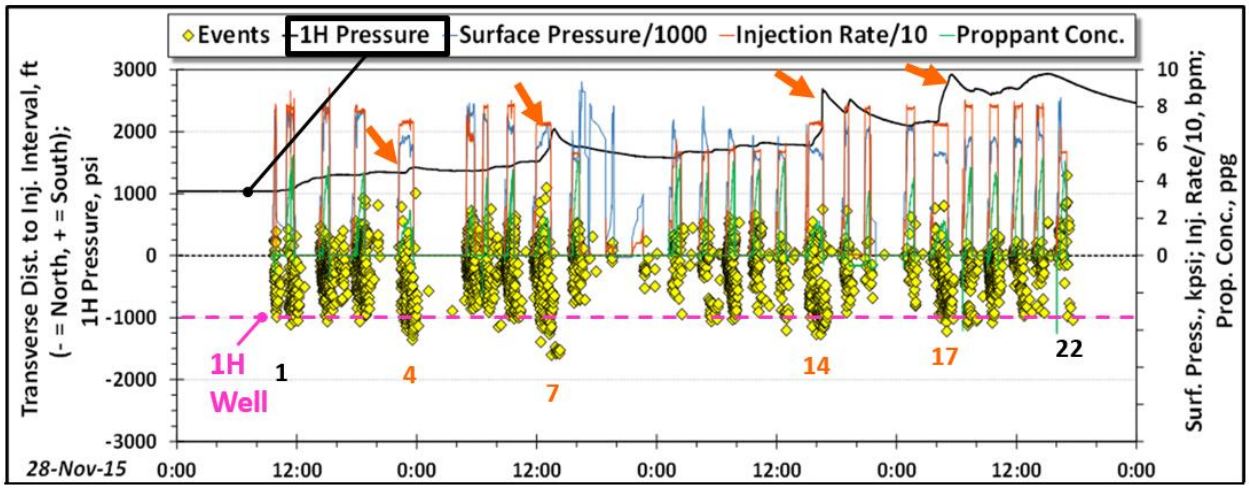

Figure 17: Example of pressure response on parent well, and its Signiant response to slick water treatments vs hybrid stages. Each orange arrow is a slickwater stage showing much greater well interference

Design A consisted of a hybrid design with larger proppants, while design B used slickwater with smaller size proppants. In Figure 17 the pressure response in the 1H well is displayed along with the microseismic events from each stage. The slickwater (design B) stages consistently showed higher magnitude pressure responses in the parent well, along with extended microseismic event clouds in the parent well vicinity. The sharp pressure responses during the slickwater stages can be characterized as frac interactions and thus have an implied longer hydraulic length. All other crosslink gel stages displayed a much slower and gradual pressure increase, which can be described as a fracture shadow pressure response from fracture overlap, not intersection, and can be implied to have shorter lengths. This case study was presented to show an obvious and measured difference in resulting fracture interference magnitude from varying completion designs on infill wells and the ability to deduce conclusions from pressure measurements.

3.5 Discussion of Present Status and Unresolved Issues

As can be seen from the literature review, many operators have experienced and are currently experiencing issues with fracture driven interaction, and it is becoming a more common

occurrence as fields mature. There is a general industry consensus that the main drivers of fracture interference between parent and child wells is manifested in the pressure gradients observed in depleted reservoirs, reduced pressure and stress, typically large completion job volumes, and modern day well spacing. The industry has developed technology to discern between direct frac hits and poroelastic responses. Additionally, these well to well signals are being used to estimate fracture properties like fracture height, length, and azimuth. Methods to determine and quantify production losses and forecast future performance have been investigated. Advanced modeling has also incorporated fully coupled poroelastic simulators to capture this phenomenon of parent well depletion and offset child stimulations.

As can be seen from the work by Miller (2016), Primary wells in various basins respond differently to frac hits and infill drilling. These parent wells represent hundreds of millions of dollars in value for the oil industry and protecting these reserves will be in the best interest of the global economy.

It has been observed that the complexity of the existing commercial models is ever increasing with new features and developments. I would suggest that the industry has far too many complex models that take years to learn or master, and far too few easy, toolbox style approaches for data analysis and modeling. Future work should include fast analytical predictions that are readily available to stream with live pressure data during fracturing operations. This way, one can make diagnostics on the fly if the fracture is propagating according to theory or if it departs from expected trends. Edits to the design can be made without the use of fully numerical solvers that can take massive computing power. Real time assisted fracture design can also help mitigate potential fracture hits. If an engineer has the observations in the field, a simple logic flow or algorithm can give assisted design input for rate variations, diverter slugs, or even next stage design changes. It can be considered a systematic method for adjustments in real time.

As noted in the literature above, there are many companies exploring the mitigation of frac interference and depletion induced underperformance of child wells. Continued work is necessary

to develop an industry standard design philosophy in this space. There are billions of dollars on the line, and this topic cannot be ignored in future research.

Fracture driven communication is an increasingly important topic to the industry, with interest growing exponentially as major US unconventional plays begin infill development phases. Fractures extending from an active well to a passive well are an expected occurrence today and are becoming part of the normal workflow for field development and optimization. The industry is in the early phases of understanding the true root causes of degraded production and is working on techniques to measure and mitigate these effects. There are quite a few areas for improvement, including fast analytical solutions and real time capability to reduce and alter fracture designs on the fly. All will help preserve the value remaining in parent wells, improve child well infill performance, and optimize full field development results.

Chapter 4. Model Development

A model description is provided along with the development and derivation of the proposed analytical model. It should be noted that this chapter samples from previously published work of the author.[2]

4.1 3D STRESS SHADOW

The new analytical model uses the fundamental equations for simple fracture geometries (KGD and PKN) and captures critical characteristics observed in field pressure interference observations. Previous discussion and detailed derivation of the analytical model used was originally published by Manchanda et al (2019) and Elliott et al. (2019). A major limitation of previous 2-D, plane-strain stress models is the assumption of infinite height fractures or infinite length fractures and over-prediction of the stress shadow perpendicular to the fracture face for very long frac lengths. Several observations from the field have shown that fracture height growth is restricted more than fracture length growth and such cases require a fixed height analytical model. Using a 2-D model in these scenarios can thus over-predict the induced stress and will not provide any diagnostic information about the fracture height in stacked or staggered development scenarios.

Stress Shadow of a 2-D Fracture

For a line crack that is opened by a constant net pressure inside the fracture, the stress shadow of that fracture is defined by the following equations:

$$\Delta\sigma_{xx} + \Delta\sigma_{yy} = -2P_{net}\left[\frac{r}{\sqrt{r_1 r_2}}cos\left(\theta - \frac{\theta_1 + \theta_2}{2}\right) - 1\right] \quad (2)$$

2 The original derivation of this model was presented at ARMA in 2019
Manchanda, R., B. Elliott, and M. M. Sharma, "Interpreting Inter-Well Poroelastic Pressure Transient Data: An Analytical Approach", 53rd US Rock Mechanics / Geomechanics Symposium, New York, New York, U.S.A., June 23-26, 2019, American Rock Mechanics Association, 06/2019.

$$\Delta\sigma_{yy} - \Delta\sigma_{xx} =$$

$$-2P_{net}\left[\frac{rsin\theta}{X_f}\left(\frac{X_f^2}{r_1 r_2}\right)^{\frac{3}{2}}\sin\left(\frac{3}{2}(\theta_1+\theta_2)\right)\right] \tag{3}$$

$$\Delta\sigma_{xy} = P_{net}\frac{rsin\theta}{X_f}\left(\frac{X_f^2}{r_1 r_2}\right)^{\frac{3}{2}}\cos\left(\frac{3}{2}(\theta_1+\theta_2)\right) \tag{4}$$

Assuming that the principal stress directions in the reservoir are aligned in the x and y directions before fracturing, we can evaluate the new state of stress in the reservoir using the following equations:

$$\begin{aligned}\sigma_{yy} &= \sigma_{hmin} + \Delta\sigma_{yy}\\ \sigma_{xx} &= \sigma_{hmax} + \Delta\sigma_{xx}\\ \sigma_{xy} &= \Delta\sigma_{xy}\end{aligned} \tag{5}$$

The opening of the fracture alters the principal stress directions. The principal stresses of the current system of equations can be evaluated and are shown in Eq. (6).

$$\sigma_{1,2} = \frac{\sigma_{xx} + \sigma_{yy} \pm \sqrt{\left(\sigma_{xx} + \sigma_{yy}\right)^2 + 4\sigma_{xy}^2}}{2} \tag{6}$$

The volumetric stress shadow induced by a 2-D fracture can be then calculated using the below equation.

$$\begin{aligned}\Delta\sigma_V &= \frac{\sigma_1 + \sigma_2}{2} - \frac{\sigma_{hmin} + \sigma_{hmax}}{2}\\ &= P_{net}\left[1 - \frac{r}{\sqrt{r_1 r_2}}cos\left(\theta - \frac{\theta_1 + \theta_2}{2}\right)\right]\end{aligned} \tag{7}$$

Stress Shadow of a Constant Height Fracture

Nordgren (1972) has shown that the width profile of a constant height fracture along the length of the fracture can be estimated using Eq. (8).

$$\phi\left(\frac{x}{X_f}\right) = \frac{w(x)}{w_{max}}$$

$$= \left[\frac{x}{X_f}\sin^{-1}\frac{x}{X_f} + \left(1 - \left(\frac{x}{X_f}\right)^2\right)^{\frac{1}{2}} - \frac{\pi}{2}\frac{x}{X_f}\right]^{\frac{1}{4}} \quad (8)$$

Additionally, the fracture width at the wellbore is given by Eq. (9).

$$w_{max} = \frac{2P_{net}h(1-\nu^2)}{E} \quad (9)$$

For scenarios in which the fracture length is much larger than the fracture height, we can assume the fracture geometry to be a sequence of several 2-D fractures arranged alongside each other from the wellbore to the fracture tip as illustrated in Figure 18. This is similar to the representation of a PKN fracture as discussed in Nordgren (1972). However, the calculation of the stress shadow induced by the PKN fracture has not been discussed in previous work.

The width of a 2-D fracture is a function of the net pressure of the fracture as shown in Eq. (10).

$$w_{max} = \frac{4P_{net}X_f(1-\nu^2)}{E} \quad (10)$$

Combining Eq. (7) and Eq. (10), we see that the volumetric stress shadow in the plane of a 2-D fracture can be expressed in terms of the maximum width of the 2-D fracture as shown in Eq. (11).

$$\Delta\sigma_V = \frac{w_{max}E}{4X_f(1-\nu^2)}\left[1 - \frac{r}{\sqrt{r_1 r_2}}cos\left(\theta - \frac{\theta_1+\theta_2}{2}\right)\right] \quad (11)$$

Now, realize that the w_{max} in Eq. (11) is the maximum width of each 2-D fracture cross-section along the length of the fracture with $X_f = h/2$. Thus, we can now transform Eq. (11) to yield Eq. (12) where $r', r_1', r_2', \theta', \theta_1', \theta_2'$ are transformed appropriately into the new coordinate system. This is visualized in Figure 18 and Figure 19.

$$\Delta\sigma_V(x,y,z) = \frac{w(x)E}{2h(1-\nu^2)}\left[1 - \frac{r'}{\sqrt{r_1{}'r_2{}'}}cos\left(\theta' - \frac{\theta_1{}' + \theta_2{}'}{2}\right)\right] \tag{12}$$

$$= \frac{w(x)E}{2h(1-\nu^2)}g(y,z)$$

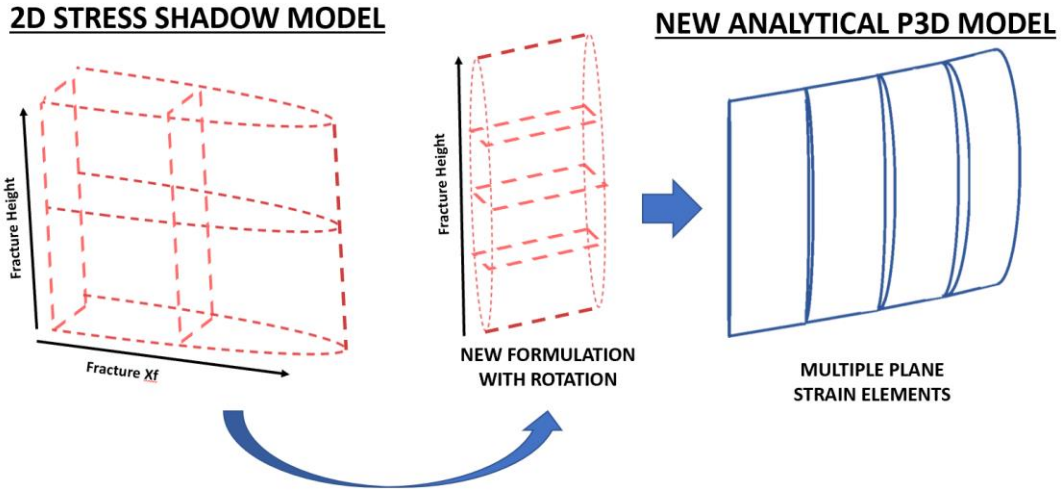

Figure 18: Transformation of a 2-D fracture to plane strain elements in a 3-D fracture

Combining Eq. (8) and Eq. (12) we can calculate the 3-D distribution of the change in volumetric stress along the length of the hydraulic fracture.

$$\Delta\sigma_V(x,y,z) = P_{net}\phi\left(\frac{x}{X_f}\right)g(y,z) \tag{13}$$

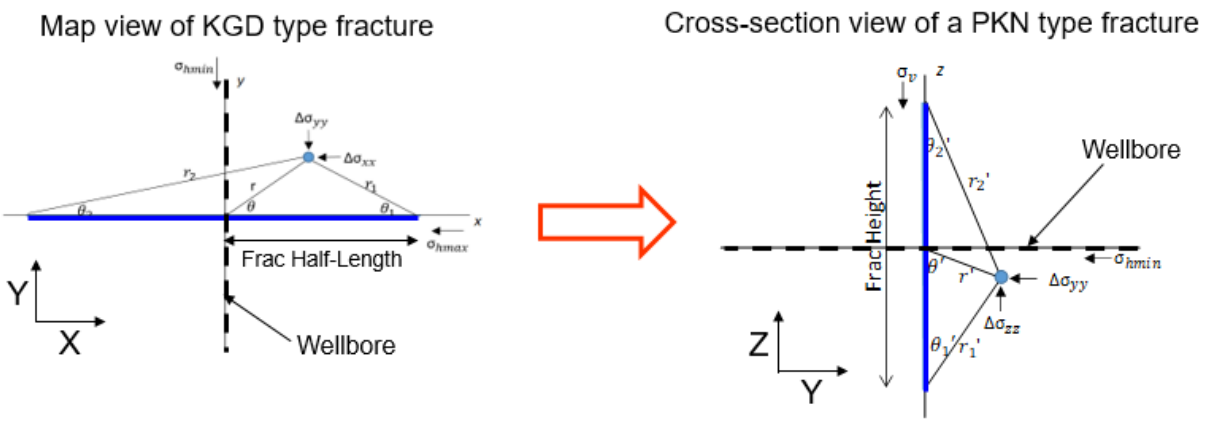

Figure 19: Coordinate Transformation

Thus, the model can be used to analytically predict the pressure change observed in monitoring well gauges using the Skempton coefficient:

$$\Delta P = B\Delta\sigma_V \ldots\ldots\ldots\ldots\ldots\ldots \text{Eq 14}$$

One of the major differentiators in the new model is the ability to capture stresses above and below the fracture, as shown in Figure 20.

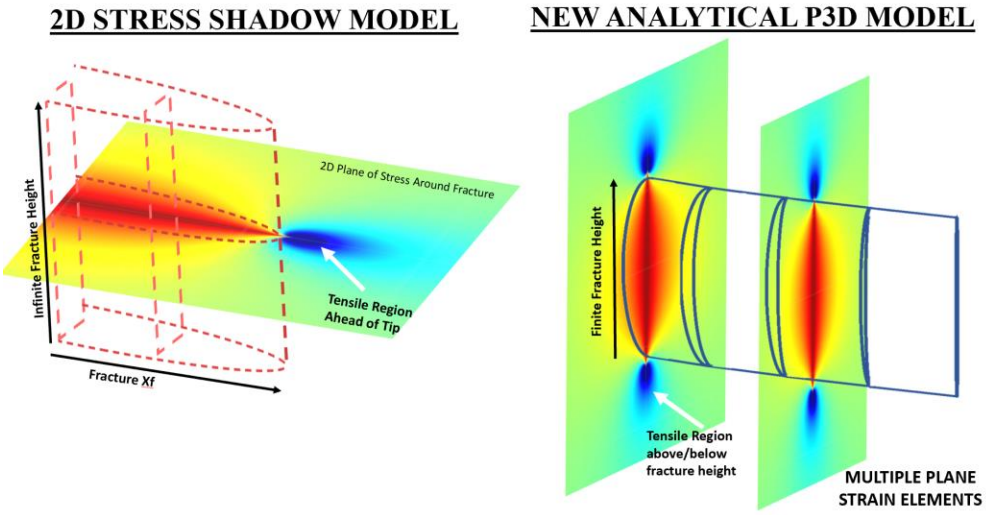

Figure 20: 2D Stress Shadow vs P3-D Stress Shadow

Multiple field stages with offset pressure responses were captured from bottom-hole gauges, interpreted, and detailed in this study. It is important to note that the current application

to the model's predicted stress in the reservoir can be related to the observed measured pressure on an externally installed casing pressure gauge, which has been perforated to the reservoir and isolated from the inner casing operations. This pressure gauge measurement can be taken as a direct known point in space, and thus volumetric stress can be backed out of the measurement at the gauge location due to a propagating offset fracture. This is different than with the existence of a monitor fracture as cited by (Kempfer 2016, Roussel 2017).

4.2 MAJOR ASSUMPTIONS

The major assumptions are as follows:

1. Stress shadow from plane strain elements along the fracture length do not interfere with each other. Considering the fracture as a PKN-type fracture, it is discretized into several plane strain elements along its fracture length.
2. Stress shadow induced ahead of the fracture tip is not calculated using this model. Using the 2-D model to calculate the stress shadow ahead of the fracture tip (in the length direction) is recommended.
3. The P3-D model results depend on the fracture height while the 2-D model results assume plane strain in the height direction and a constant width along the height of the fracture.
4. The P3-D model considers a variation in the pressure distribution in the fracture (and thus varying width) while the 2-D model assumes a constant net pressure in the fracture.
5. The 2-D model considers the impact of the stress shadow induced by locations along the fracture length on each other. The P3-D model uses the plane strain approximation in the fracture length direction and disassociates the impact of stress shadow induced by plane strain elements on each other. This assumption will be validated in later work using 3-D fully coupled poroelastic numerical simulations.

4.3 A COMPARISON OF 2D AND 3D STRESS SHADOWS

A 2-D fracture is a line crack that does not have a height dimension. Figure 21 and Figure 22 show the volumetric stress shadow induced by a 2-D fracture using Equations (7). The results show the volumetric stress changes in the reservoir both perpendicular to the fracture as well as ahead of the fracture tip. The green line in Figure 22 marks the boundary region between the compressive and tensile stress shadow regions. Note that these regions are independent of the in-situ stress values and the height of the fracture and the model assumes a constant fluid pressure in the fracture (which is a major limitation this work attempts to overcome using the Nordgren width and pressure change along the fractures length).

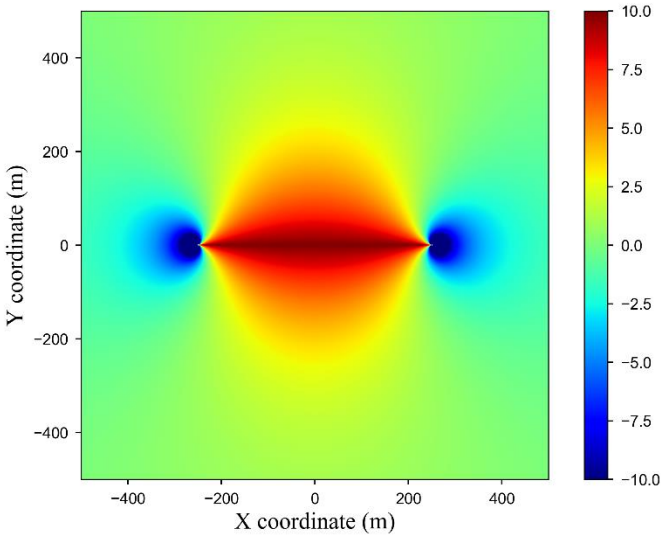

Figure 21: Surface plot of volumetric stress shadow (in MPa) induced by a 500 m long fracture at a constant internal net pressure of 10 MPa. The fracture is centered at (0, 0) and is parallel to the X axis. Stress shadow is calculated using Eq. (1)

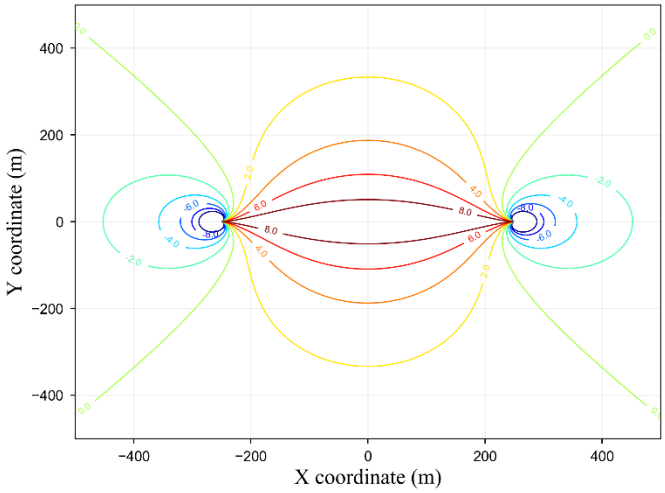

Figure 22: Contour plot of volumetric stress (in MPa) induced by a 500 m long fracture at a constant internal net pressure of 10 MPa. The fracture is centered at (0, 0) and is parallel to the X axis. Stress shadow is calculated using Eq. (1).

In order to include the impact of fracture height, the P3-D model was developed in this work as discussed **Error! Reference source not found.**. Figure 23 compares the results from Equation (7) and Equation (13). As expected, comparing the 2-D model with the P3-D model shows significant differences in the results. These differences are caused by the following primary differences between the models:

1. The P3-D model results depend on the fracture height while the 2-D model results assume plane strain in the height direction and a constant width along the height of the fracture.
2. The P3-D model considers a variation in the pressure distribution in the fracture (and thus varying width) while the 2-D model assumes a constant net pressure in the fracture.
3. The 2-D model considers the impact of the stress shadow induced by locations along the fracture length on each other. The P3-D model uses the plane strain approximation in the fracture length direction and disassociates the impact of stress shadow induced by plane strain elements on each other. This assumption will be validated in later work using 3-D fully coupled poroelastic numerical simulations.

One feature of the 2-D model that is not possible in the presented P3-D model is the calculation of stress changes ahead of the fracture tip in the length direction. The tensile stress

shadow iduces by a 2-D fracture is not a strong function of the fracture height, so it is recommended to use the 2-D model to estimate the tensile stress shadow ahead of the fracture tip. Also, the P3-D model is only applicable in scenarios where the fracture height is a constant value for the entire fracture and is much smaller than the fracture half length. This is a common constraint in unconventional fracture geometries. Though the model can be easily extended to scenarios where the height may vary along the length of the fracture, analytical representation of the fluid pressure in the fracture is not available. Such extension will require coupling of the presented model with numerical evaluation of the pressure drop along the fracture length direction. This will be discussed in future work.

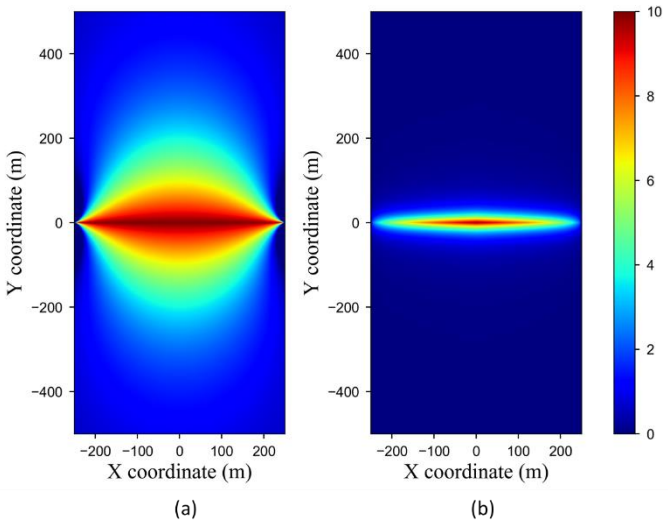

Figure 23: (a) Volumetric stress shadow induced by a 2-D fracture (b) volumetric stress shadow induced by a 3d fracture that is 50 m tall on a horizontal plane through the middle of the fracture (centered at 0,0,0).

4.4 MONITOR WELL GAUGE PRESSURE RESPONSE

The stress shadow induced by a propagating fracture can alter the pore pressure in the reservoir. A solution of the poroelastic equations to determine these changes can be done numerically (Manchanda 2015). This work uses a simplified poroelastic model as shown in Eq. (15).

$$\Delta P = B\Delta\sigma_V \quad (15)$$

B in the above equation is the Skempton coefficient (Roussel and Agrawal 2017). This coefficient depends on the compressibility of the fluids in the reservoir and the compressibility of the mechanical structure of the formation. One can use different values of B to understand the impact of this poroelastic pressure change for both oil and gas reservoirs. This model calculates the pressure change induced at any point in the reservoir because of the volumetric stress change calculated by the stress shadow models. This can also be used as a field history matching parameter, as measuring Skemption coefficient is difficult in low permeability core samples.

Using the analytical model to begin to predict the volumetric stress, with pressure changes expected around a fracture as a function of varying input parameters is discussed below. Figure 24(left) below shows the effect of varying height on the predicted response, from 25m fracture height to 150m fracture height in increments of 25 meters. This result obviously shows the degradation expected with increase perpendicular distance from the fracture face, and as expected, increase fracture height yields a wider width at a fracture's origin and a larger observed pressure change away from the fracture. Figure 24 (right) displays the variability on P_{net} and the pressure change associated from an elastic response ranging from 1 MPa to 11 MPa (or 145 psi to 1,595 psi). With additional P_{net} in the fracture, higher pressure changes at given distances from the fracture can be seen, this relationship is critical for calibrating a stimulated stage's net pressure and expected responses.

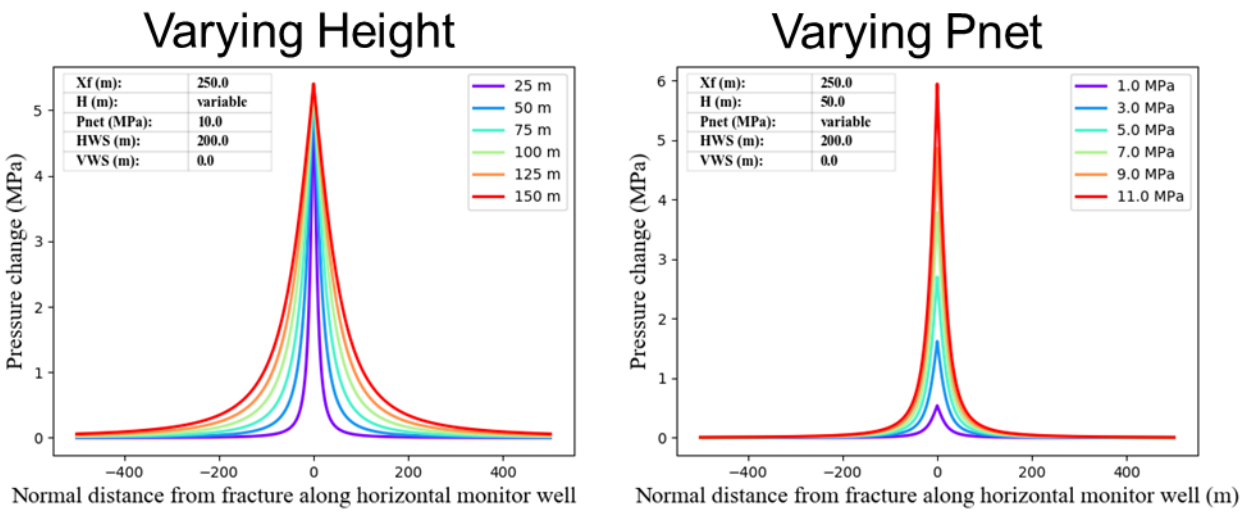

Figure 24: Displays of analytical model predictions and calculated pressure changes normal to the fracture face along a horizontal plane

The volumetric stress shadow induced by a finite height fracture was introduced above. A pressure gauge in a well near an open hydraulic fracture shows a pressure signature corresponding to a propagating fracture. This pressure signature is induced by the poroelastic coupling of the stress shadow generated by a propagating fracture and the pressure changes in the reservoir.

4.5 Model Schematic for Field Application

It is prudent to describe the various geometries and fracture schematics that can be represented by this model. As mentioned previously, calculating estimates of stress above and below a propagating fracture was not possible with existing formulations. In modern unconventional reservoirs, it is common and expected to have multiple horizontal wells stacked or staggered in development patterns. As can be seen by Seth et al. (2019) the application of in-zone or same layer calculations are limited and not feasible in this scenario, and use of our model would be required for this case. The results that will be described in the remaining sections will consist of a propagating fracture and expected pressure measurement at various points along an offset wellbore (Figure 25).

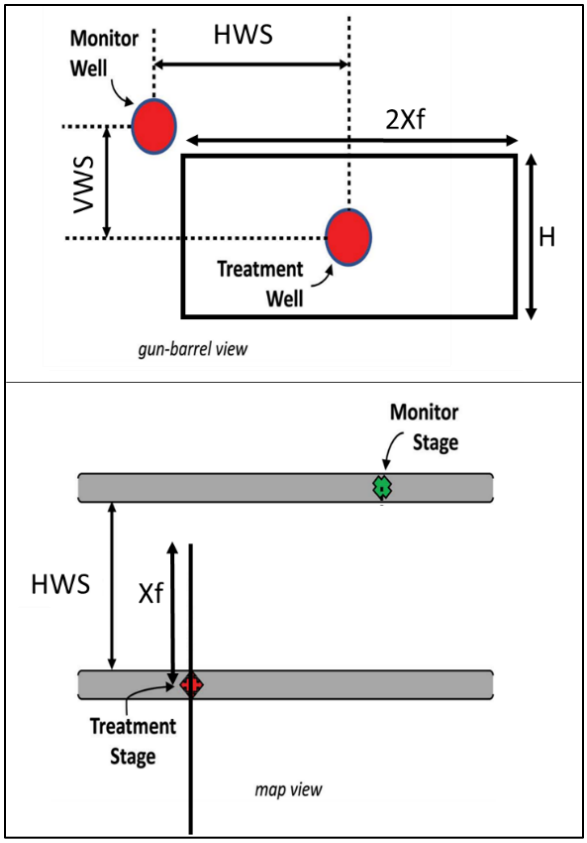

Figure 25: Schematic showing spatial configuration of treatment and monitoring well pair. HWS stands for Horizontal Well Spacing, VWS stands for Vertical Well Spacing, Xf refers to fracture half-length and H refers to the fracture height (modified from Seth et al)

Chapter 5. Modeling Sensitivities and Validation

This section describes the sensitivity analysis of the P3-D model across a broad spectrum of input data, in order to understand potential pressure responses expected in the field. This sensitivity uses a comprehensive range of parameters that is estimated from other fracture diagnostics and personal industry experience. The numerical validation is necessary to baseline the new P3-D model with existing fully coupled geomechanical fracture simulations.

5.1 RESULTS GIVEN VARIOUS VARYING PARAMETERS

The base case parameters used in this analysis are shown in **Error! Reference source not found.**. In this analysis, each of the parameters are varied, and the pressure change (Y axis value) at various locations along a monitoring horizontal well (X axis value) is calculated. The sensitivities analyzed for all cases are shown in **Error! Reference source not found.** and are also shown as the legend values in Figure 26 – Figure 32. In this analysis the value of Skempton coefficient used is 0.9. This value can be changed to consider the impact of different formation properties such as rock bulk modulus and the fluid compressibility.

Parameter	Base	Sensitivities
Xf (m)	250	205, 225, 250, 275, 300
H (m)	50	25, 50, 75, 100, 125, 150
Pnet (MPa)	10	1, 3, 5, 7, 9, 11
HWS (m)	200	0, 50, 100, 150, 200, 245
VWS (m)	0	0, 12.5, 25, 37.5, 50

Table 1: Base Case Parameters for Sensitivities

Figure 26 shows the impact of fracture length on the pressure change observed along a monitoring horizontal well. Only scenarios in which the horizontal well spacing is less than the fracture half-length were considered to ensure compatibility with the assumptions of the 3-D model. The results show that as the fracture grows longer, the pressure change at the monitoring

well gauge location increases. This is because a longer fracture leads to a greater fracture width at the location of the monitoring well. The pressure change decays very rapidly along the monitoring well within the first 100 m away from the fracture. For a monitoring pressure gauge 40 m away from the fracture a 225 m fracture would induce a pressure change close to 0.66 MPa while a 300 ft fracture would induce a pressure change close to 1 MPa. This strong dependence of the pressure changes on the fracture half-length can be very useful when interpreting fracture geometry from the observed monitoring pressure data, as shown in the next section.

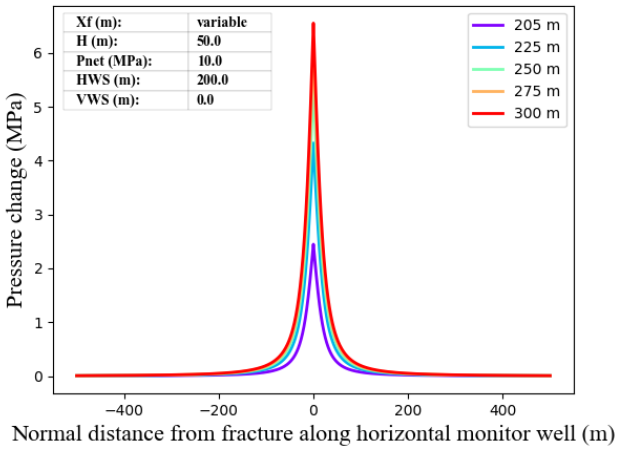

Figure 26: Impact of fracture length on pressure change observed in a horizontal pressure monitoring well.

Figure 27 shows the impact of fracture height on the observed pressure changes in the monitoring well pressure gauge. This figure presents the novelty of using a 3-D model to interpret the observed pressure change in the monitoring well. As discussed above, 2-D models do not consider a height dimension and as such do not provide diagnostic information about the fracture height. The analysis presented in Figure 28 shows that the pressure change observed is significantly affected by the fracture height. Thus, observing the pressure change in the monitoring well can provide firm diagnosis of the fracture height by using the presented model.

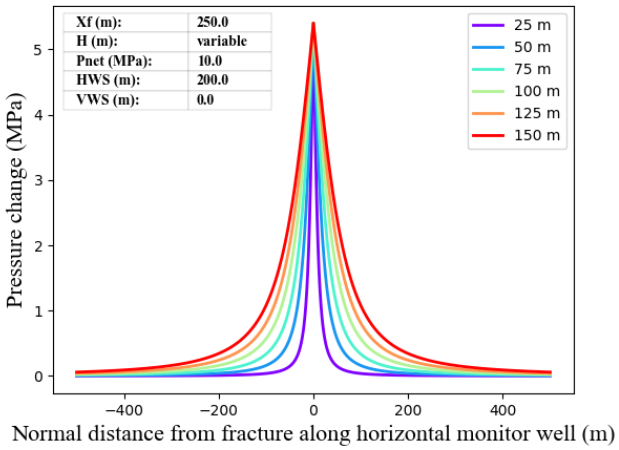

Figure 27: Impact of fracture height on pressure change observed in a horizontal pressure monitoring well.

The net pressure specified in in Figure 26-Figure 29 is the value calculated using the fracture pressure and the reservoir minimum principal stress near the mouth of the propagating fracture (where the fracture meets the wellbore). The pressure drop from the mouth of the fracture to the tip of the fracture in the length direction is considered in the model and is described in the Appendix. Figure 28 shows the impact of net pressure on the monitoring well pressure response. It is evident from the figure that the magnitude of the observed pressure change is a strong function of both the input net pressure and the distance of the monitoring well pressure gauge from the fracture. The observed pressure change is directly proportional to the net pressure, which means that an increase in the net pressure by a factor leads to an increase in the pressure change by the same factor. In most situations, the net pressure value fracture very near the wellbore can be estimated from the well design, completion design, treatment parameters, and knowledge of the surface pressure in the treatment well. Therefore, we consider the net pressure as a known parameter in the system and can use it to estimate the induced pressure changes in the monitoring wells.

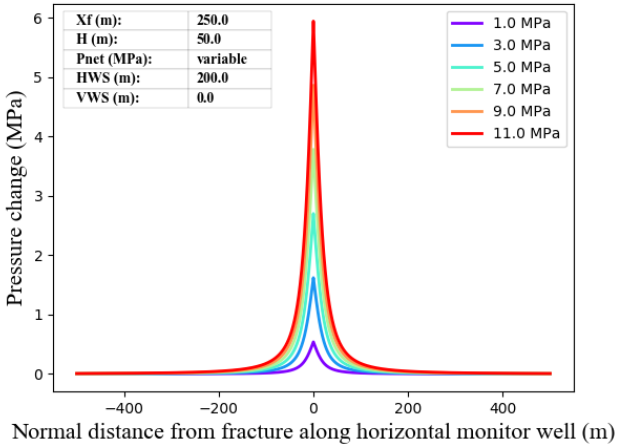

Figure 28: Impact of fracture net pressure on pressure change observed in a horizontal pressure monitoring well.

Figure 29 shows the impact of horizontal well spacing on the observed pressure change in the monitoring well. Seth et al. (2018) have shown that the fracture length and the horizontal well spacing have complementary effects on the observed pressure change. They use the overlap length between a fracture and the monitoring well to suggest this.

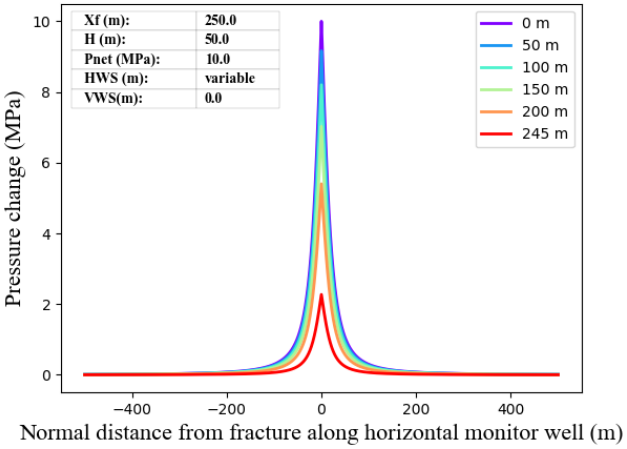

Figure 29: Impact of horizontal well spacing on pressure change observed in a horizontal pressure monitoring well.

Figure 30(a) shows a zoomed in view of Figure 29 where the horizontal well spacing was varied for a constant fracture length. Figure 30(b) shows a scenario where the overlap distance is kept constant at 250 m and both the fracture half-length and horizontal well spacing are varied. Unmistakably, plotting the pressure change as a function of overlap distance helps normalize the effect of fracture half-length and the horizontal well spacing.

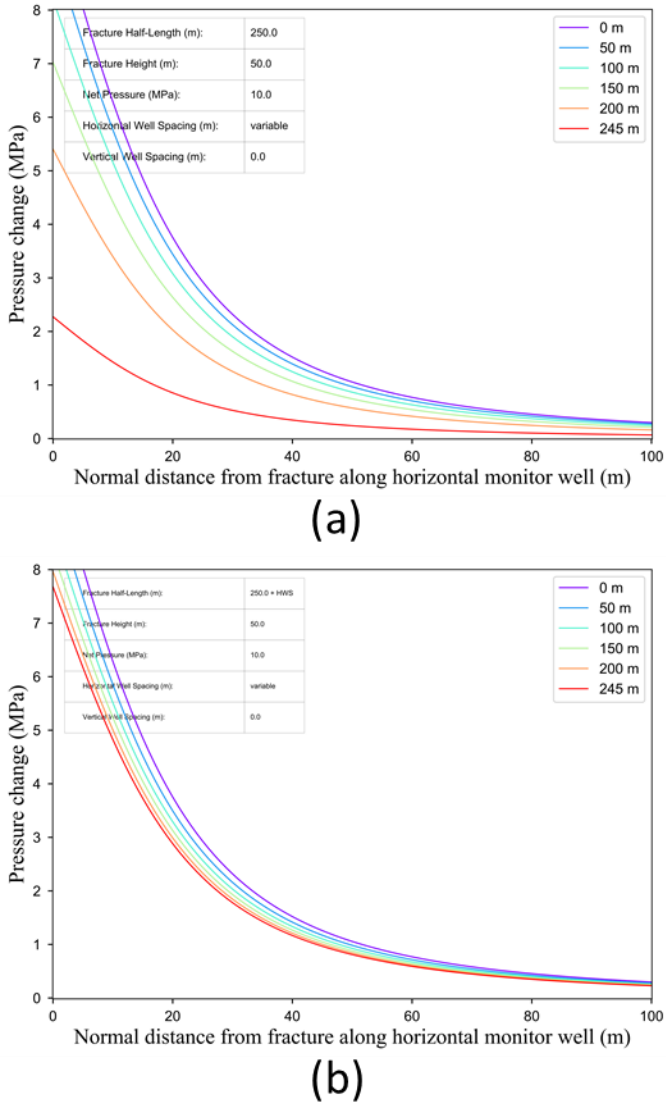

Figure 30: (a) Zoomed-in view of Fig. 12. (b) Zoomed-in view of the pressure change vs distance from fracture as a function of the overlap distance between the fracture length and the horizontal well spacing.

Figure 31 and Figure 32 depict another important and novel result from the 3-D model presented in this work. In addition to showing how the pressure changes in the monitor well change as a function of the propagating fracture height, they also portray pressure changes in a monitoring well as a function of the pressure gauge location in the vertical coordinate. The results here showcase that sharp changes in the pressure response in the monitoring well are observed when the monitoring well gauge lies above or below the fracture. The observed negative pressure change values represent the tensile region that exists ahead of a fracture tip (in the vertical direction). The observation of this tensile region is a consequence of using the 2-D model for individual plane strain elements. The impact of this observation on the interpretation of fracture height is discussed further in the section **Error! Reference source not found.**.

Figure 31: Impact of vertical well spacing on pressure change observed in a horizontal pressure monitoring well.

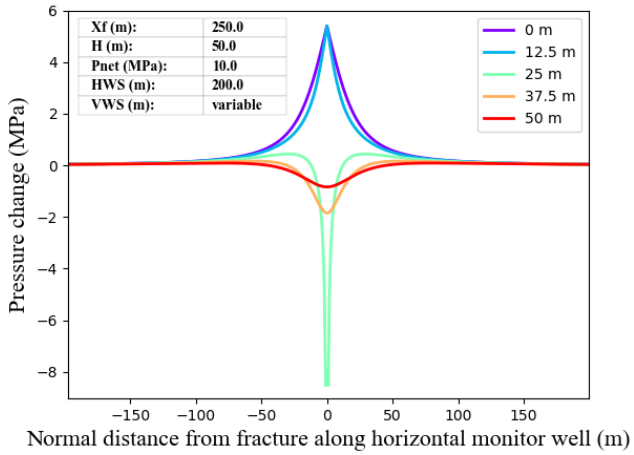

Figure 32: Zoomed-in view of the impact of vertical well spacing on pressure change observed in a horizontal pressure monitoring well.

5.2 COMPARISON BETWEEN NUMERICAL AND ANALYTICAL MODELS

To test the validity of the newly developed analytical model, a test case was developed and compared with results obtained from a fully numerical model. The numerical model used in this study has been described in significant detail previously (Manchanda et al. 2019, Seth et al. 2019, Zheng et al. 2019).

To validate the analytical model, the calculations of volumetric stress changes in the reservoir from numerical simulation were compared directly with the predictions from the analytical model. Since one of the major novel components of the analytical model was the prediction of stress at and above the fracture plane, multiple slices along the analytical fracture estimate were compared with the fully numerical result. The fracture geometry test case displayed in the paper consisted of a fracture with a height of 50 m, a half-length of 248 m, and a net pressure of 0.5e6 Pa at the wellbore. Z plane slices were compared at the origin (0 m above the origin), the top quarter of fracture (12 m above origin), at the top of fracture (24 m above origin), and 12 m above fracture top (36 m above origin). These slices represented a spread of values and showed agreement between the numerical model and the analytical model. These slices are represented in Figure 33, which displays results at the origin with a generally positive volumetric stress that

increases around the fracture, while above the fracture (bottom right), tension or negative volumetric stress change due to tip effects around the fracture itself.

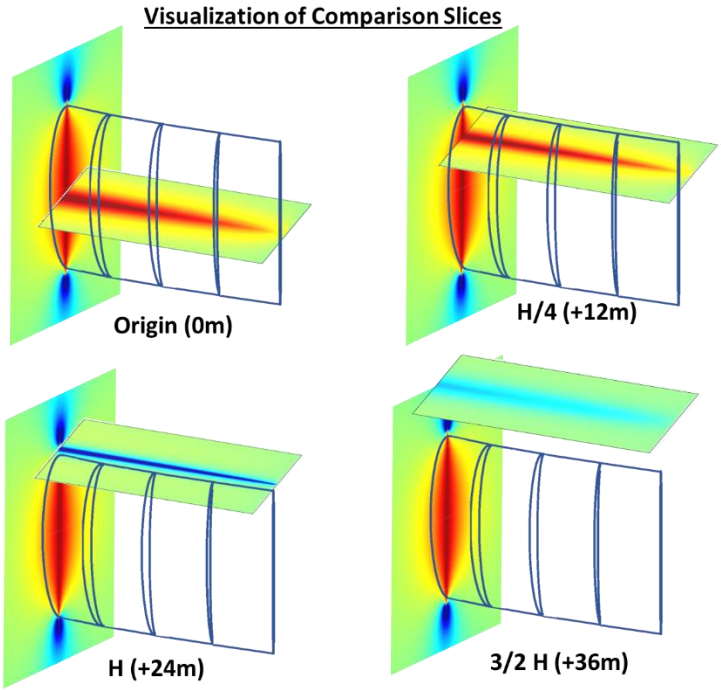

Figure 33: Slices for direct comparison between the new analytical model and fully numerical solutions.

The accuracy and error between the analytical model and the numerical model depend on gridding and grid resolution in the numerical model. The slight mismatch at the fracture origin (0 m normal to fracture face) in Figure 34 is a function of mesh refinement, specifically where the mesh transitions from fine to coarse. It is observed that with additional levels of refinement the results from the numerical approach better match with the smoother solution from this analytical model (Figure 34A fine mesh was used for up to 20 m normal distance from the fracture face and a coarser mesh used past 20 m in the numerical model. A 1 meter mesh size up to 20 m (~500,000 grid blocks) was the optimal mesh size that the computation could handle for the given dimensions of the fracture. Limitations arise in the total number of grid-cells in the numerical simulation due

to computational memory availability. Reducing the mesh size further would result in a better match with the analytical result but would require increased computational memory.

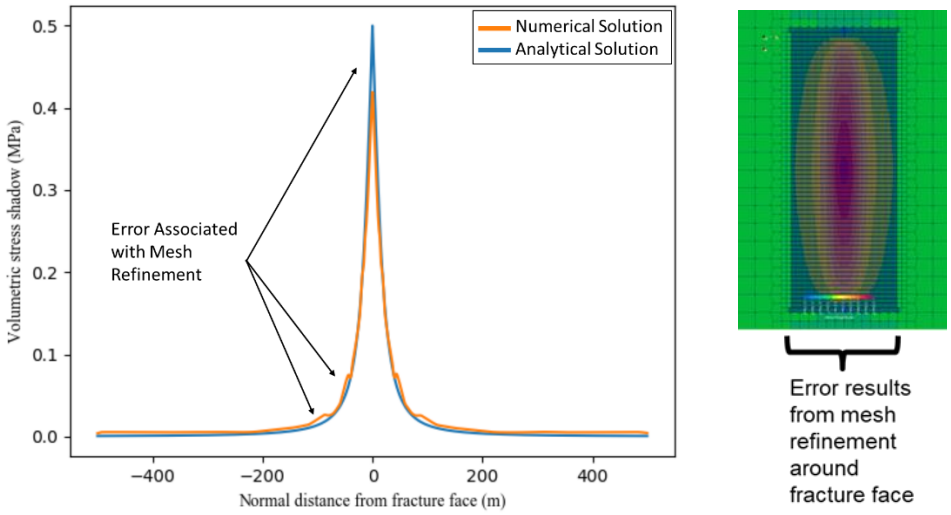

Figure 34: Volumetric Stress: Results from numerical simulation and analytical solution at the fracture origin.

5.2.1 Varying parts of fracture

Figure 35 shows a comparison between the analytical model and the numerical model. The two resulting stress fields are plotted along a surface at the fracture mid-point in Figure 35 and the incremental stress around the fracture along a plane at the origin of the fracture, which is characteristically the widest part of the fracture, is displayed. Figure 35 (right) displays the normalized error between the models as a slice along the plane at various positions along the fracture's length. Note the overall error past 30 m from the fracture is less than 2%.

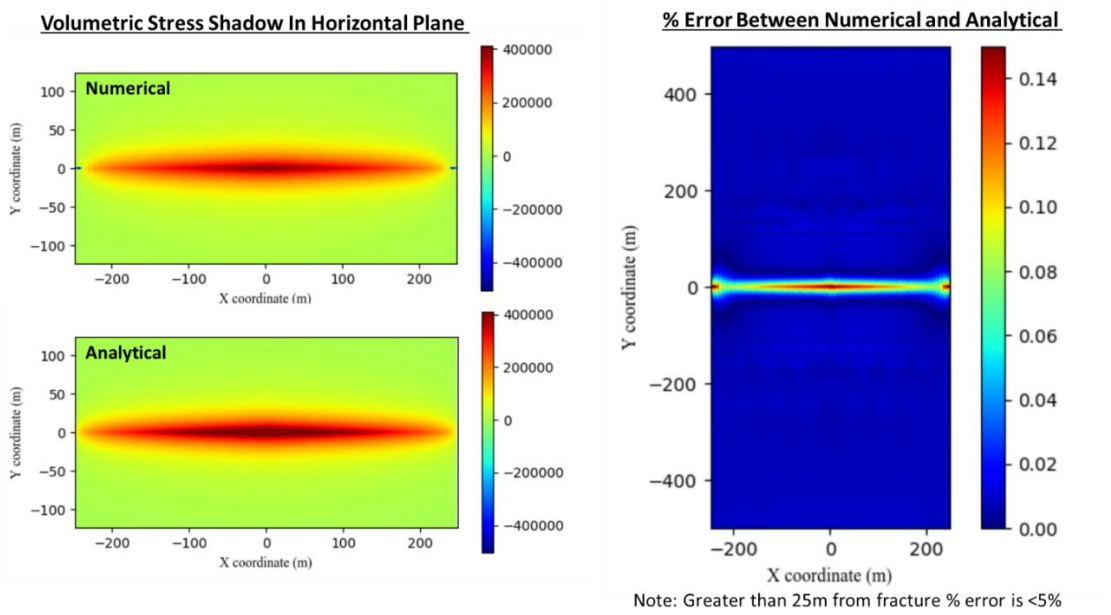

Figure 35: Comparison of numerical model volumetric stress shadow (TOP LEFT), with the newly developed analytical model (BOTTOM LEFT) Units are in Pa, and distance in meters. A % error between the two volumetric stress solutions (RIGHT) for a horizontal plane a

As can be seen in Figure 34 to Figure 36 there is very good agreement between the two model solutions. Any error between the solutions is due to the high rate of change of volumetric stress near the fracture and is purely a function of gridding in the numerical model. To put this error in perspective, we observe a tolerance of less than 5%, beyond 15 m perpendicular to the fracture face at either side, in the volumetric stress prediction.

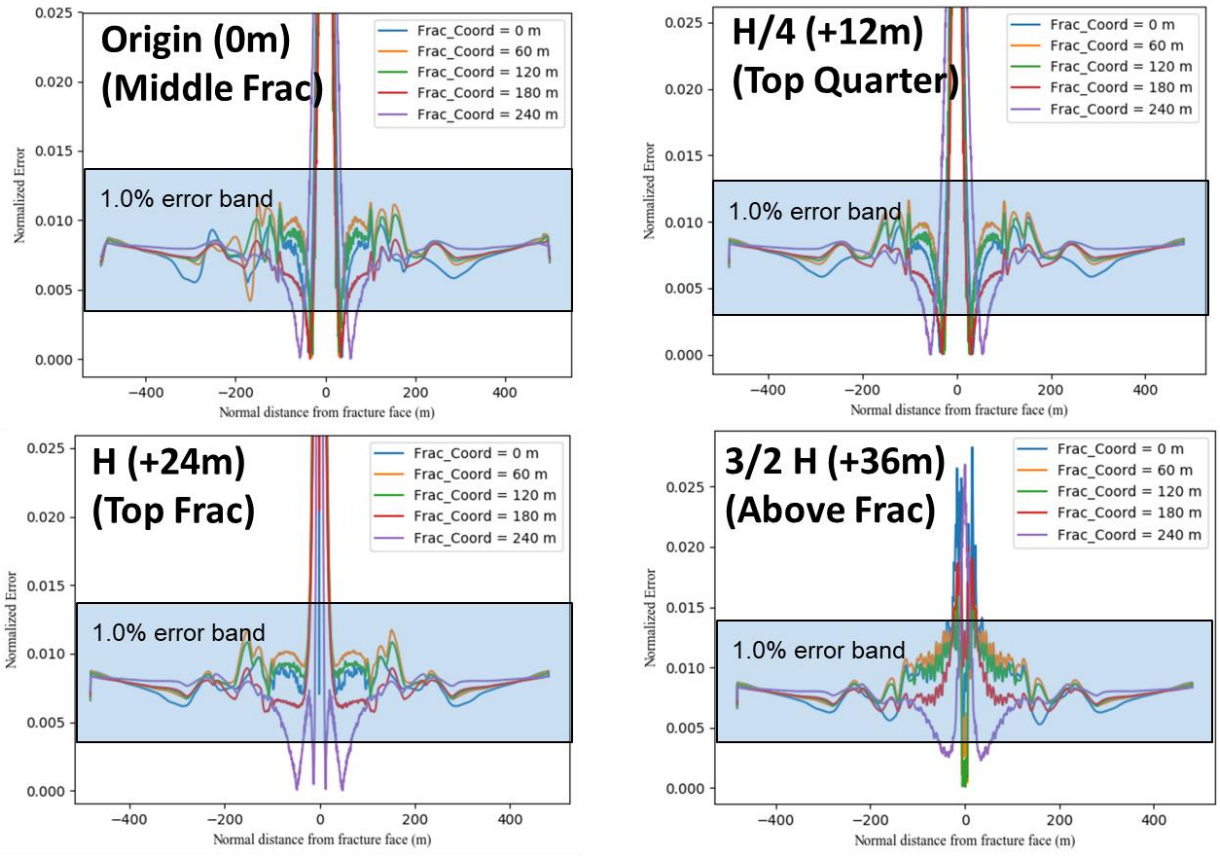

Figure 36: Resulting error in volumetric stress perpendicular to the fracture face for various slices in fracture height and along fracture length.

5.2.2 Error Discussion

Using the analytical model, we can predict the distance where an expected pressure change of 1 psi occurs (using a Skempton coefficient of 1), for a fracture with 500 psi net pressure. This occurs 1,312 ft from the fracture face. This region can be seen in Figure 37, which shows the relative error window greater than 5% (red), in contrast to the region where we expect accurate stress and pressure predictions within ~2% of the numerical model (green). It can be noted that the accurate zone covers over 50% of a typical 5,000 ft lateral. This is an additional benefit of the

analytical model as a scoping tool to plan gauge placement and observation points in the reservoir for optimal coverage.

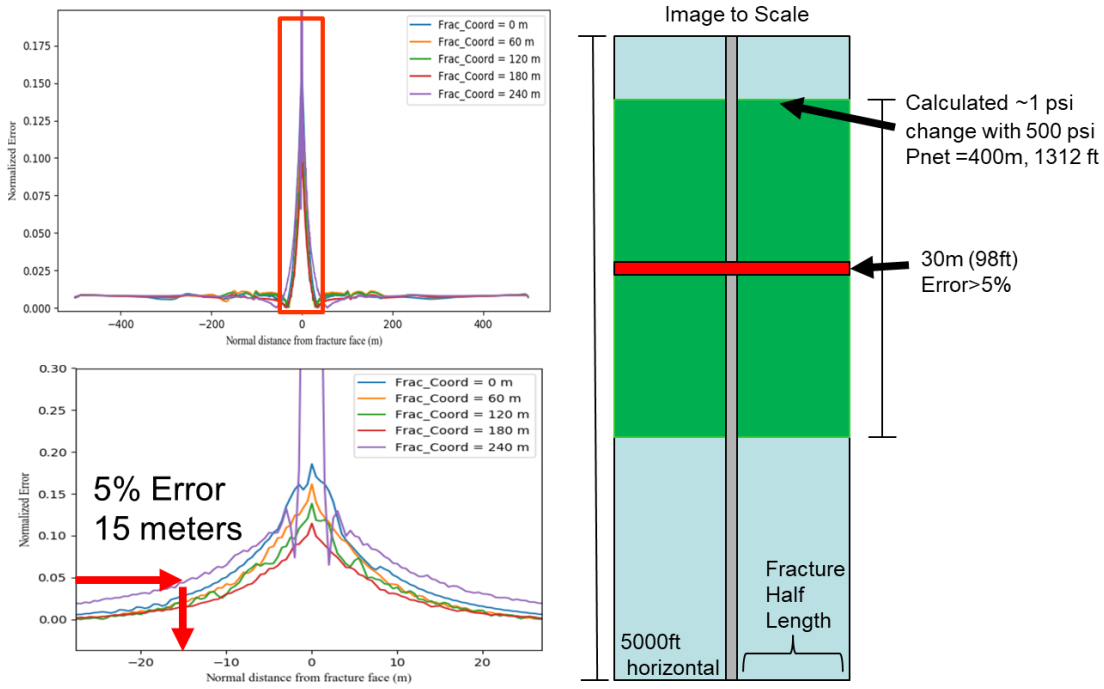

Figure 37: Region of normalized error greater than 5% is 98ft, region of accurate stress predictions (less than~2% error) is 2624 ft (52% of lateral).

As stated earlier, one of the major motivations for this work was to overcome the time and computing power limitations of full 3-D numerical modeling. Many runtimes of 3-D fracture models are time-prohibitive for rapid analysis and are typically done after the stimulation as a history match or lookback process. With this new model and workflow, stresses around a fracture are able to be estimated in less than 1 second compared to the exact same case for the numerical model of 4.5 minutes. This represents a 270-fold decrease in run time. This allows us to have the ability to run multiple cases and implement the solutions in real time or simply to have a handy process for stress estimates in the reservoir.

Chapter 6. Analytical Inversion & Resolving full Solutions

6.1 SURFACE SOLUTION

The primary unknowns in Equation (13) are the fracture half-length, fracture height, and fracture net pressure. The other parameters that are part of the equation are dependent on the distance between the wells (both horizontal distance and vertical distance) and the perpendicular distance between the fracture and the monitoring well pressure gauge. These parameter values are known and can be calculated by analyzing the directional survey of the subject wells. Using known values of these parameters, several solutions can be obtained of the fracture half-length, fracture height, and fracture net pressure. In order to obtain these solutions, the "minimize method" from the "optimize module" in the SciPy library of Python (Jones et al., 2001) was used. The built in functionality of the Sequential Least Squares Programming (SLSQP) algorithm is used to obtain the solution. A graphical way to represent these solutions is to represent them as a surface plot as shown in Figure 38. Every point on the surface satisfies the constraint of observed pressure change at the monitoring gauge for the defined well configuration.

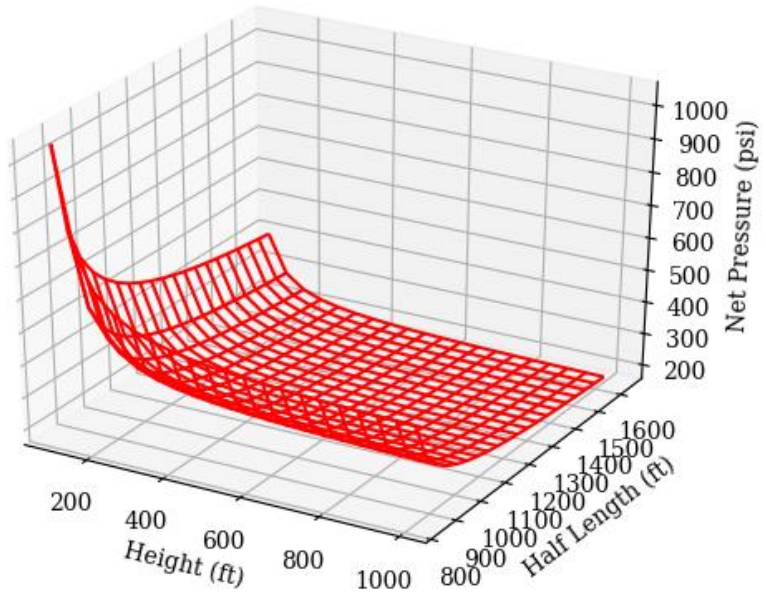

Figure 38: Example surface of solutions for a scenario where the perpendicular gauge distance from the fracture is 10 m, the observed pressure change in the monitor well gauge is 100 psi, the Skempton coefficient is 0.8, the horizontal well spacing is 800 ft

6.2 INTERSECTING PLANE METHOD FOR A 3 GAUGE SOLUTION

If there is a field scenario where multiple monitoring wells and multiple monitoring gauges are used, it will be possible to find the intersection of several surfaces to obtain a unique estimate of the length, height, and net pressure of a fracture. For example, consider the schematic shown in Figure 39, in this scenario the monitoring well gauges record the specified pressure changes for a fracture with unknown length, height, and net pressure. For the pressure response in each monitoring gauge, a surface of solutions can be obtained. The three pressure responses thus lead to three surface solutions as shown in Figure 40.

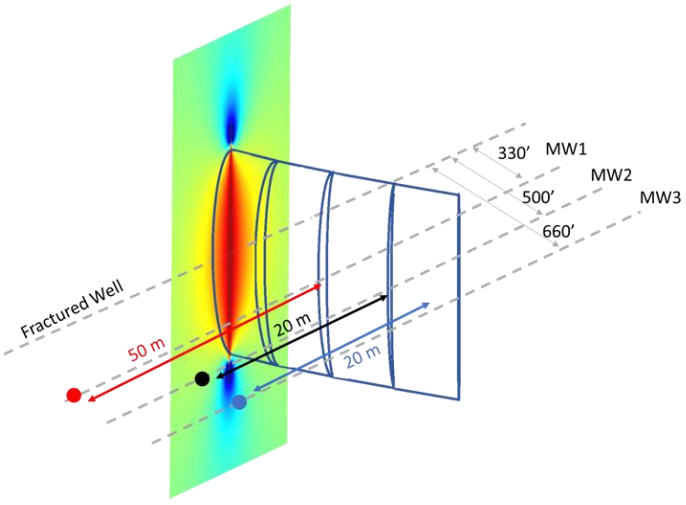

Monitoring Well	Observed Pressure Change
MW1	14 psi
MW2	36 psi
MW3	29 psi

Figure 39: Example schematic showing the location of a fracture with respect to three monitoring wells and three monitoring gauges. The table shows the observed pressure change in the three gauges.

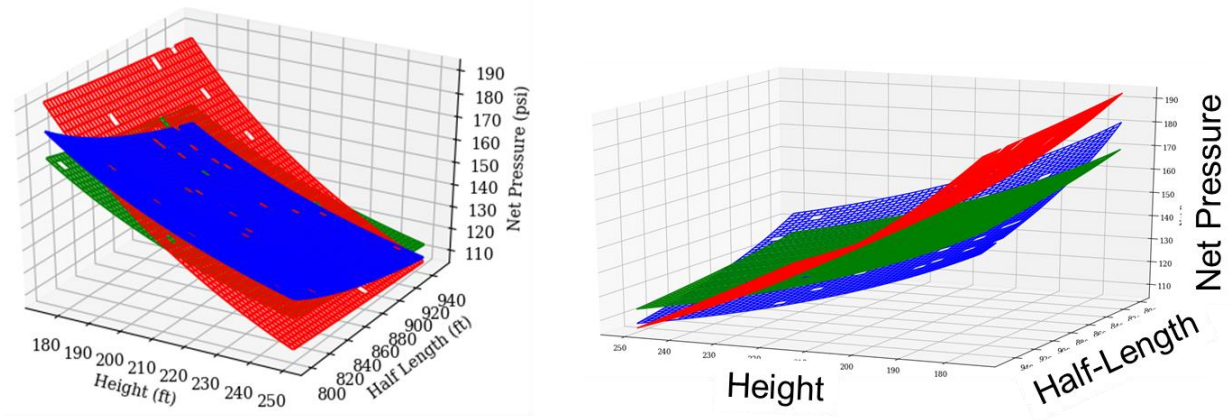

Figure 40: Intersection of three surfaces, representing the full solution for each individual gauge.

Theoretically, the three surfaces should intersect at a point to identify a unique solution. However, in reality, the reservoir system and the stress changes in the system are much more complex. The solutions may not meet at a single point. To resolve this issue, the regions where the solutions are closest to each other can be determined, rather than a single point. This is accomplished by creating an objective function that calculates the difference between the net pressure values for all combinations of length and height for each surface. This objective function for three surfaces is defined as:

$$f(X_f, H) = \log\left(\sqrt{\left(P_{net,1} - P_{net,2}\right)^2 + \left(P_{net,2} - P_{net,3}\right)^2 + \left(P_{net,3} - P_{net,1}\right)^2}\right) \ldots\ldots\ldots Eq.16$$

This objective function can be extended to include results from more surfaces by including all combinations of the differences of all the surfaces as shown below:

$$f(X_f, H) = \log\left(\sqrt{\sum_{i}^{n}\sum_{j>i}^{n}\left(P_{net,i} - P_{net,j}\right)^2}\right) \ldots\ldots\ldots\ldots\ldots Eq.17$$

The objection function described above can be plotted for the example values shown in Figure 39 for a range of fracture half-lengths and fracture heights (Figure 41). The circled region in the figure shows the region where the solution attains a local minimum. From this inversion an

estimate of the fracture height is ~220 ft, fracture half-length is ~860' and the net pressure can be calculated by using the forward model with the above values to be ~145 psi. Any uncertainty in the input pressure and variability in the known distance will cause a slight alteration in an individual surface solution, but this can be evaluated and observed by the low error intervals (blue). A field diagnostic that resolves fracture height and length within 10% accuracy is considered extremely useful for the industry.

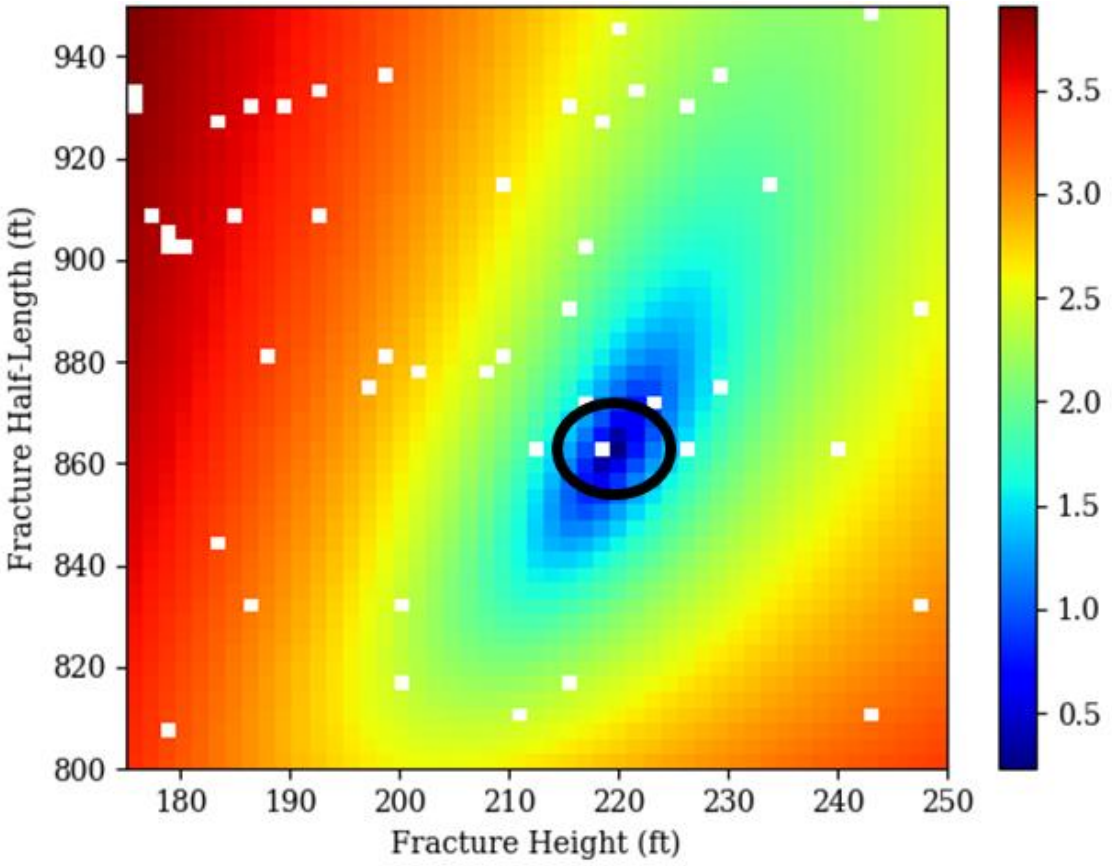

Figure 41: Objective function values shown for the model schematic in Figure 8. The white squares represent regions where the inversion was unsuccessful.

To develop an understanding of how this model can be used in real time, a pseudo-field case is simulated. As the fracture continues to grow in geometry through time, new pressure estimates are observed. A new solution is iterated upon at each time step and the fracture geometry is updated. As can be seen in Figure 42 the early time step (left) converges on a fracture geometry of 150 ft height, and 800 ft Xf. It is important to note the red portions of these images are highly unlikely values due to the mismatch between the plane solutions discussed earlier. White indicates no solution, or impossible convergence. One can note here that the no solutions are possible for a fracture less than 660 ft, which is the well spacing for this case. The fracture continues to grow and yields a final solution of 250 ft height, and 850 ft length and can be seen on the right. It is important to note that uncertainty grows with time as can be seen from the blue envelope in the image. There are more potential matches, and this yields a good visualization of the uniqueness of the solution. The gold star is depicted at the true local minimum error and resulting best inverted solution.

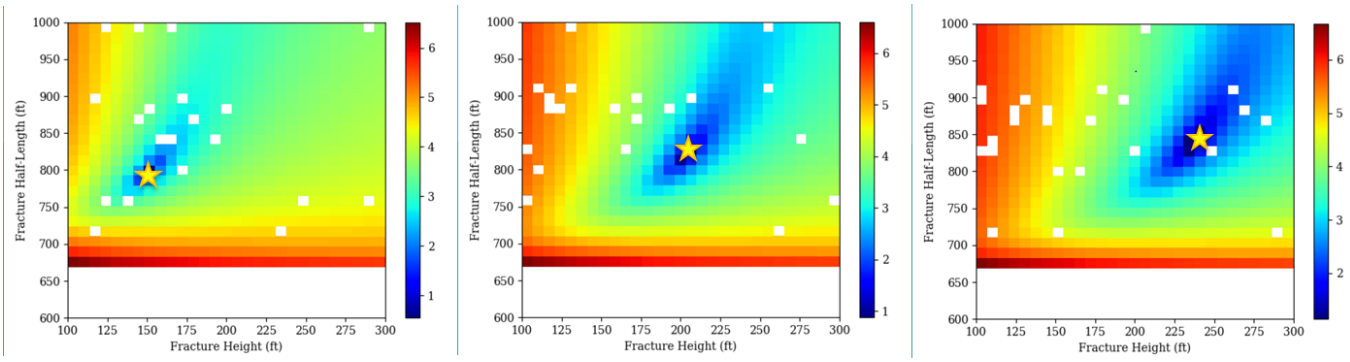

Figure 42: Solutions for fracture geometry across multiple timesteps for a pseudo-case

This inversion process helps identify the fracture dimensions for scenarios in which multiple field data sources are available. In the above example, the three data sources are the pressure changes observed in three monitoring gauges in the three wells. There are several other forms of data that could be used in this inversion process, as shown in Table 2

Data Capture	Method for Constrained Solution
Material Balance	Calibrate volume injected during fracturing stage vs volume inside fracture from inversion solution
Instantaneous Shut in Pressures	Calibrate to net pressure at end of stage
Water Hammer	Relationship between water hammer workflow and dimensions observed in pressure signal

Table 2: Additional Methods to Yield Constrained Solution

Integrated modeling of the above data sources can help in uniquely identifying the fracture geometry for a particular stage in a well. For any field experiment that does not have three external gauges in a measurable region from the fracture, the user will need the additional information described in Table 2. This is explained in detail for a field case where two gauges were available, and an additional calibration point was necessary in section 8.3 and 8.3.

Chapter 7. Modeling Field Use Cases

Figure 43 shows a field data set where the impact of pumping in a treatment well (blue) is seen as pressure changes in a monitoring well (orange). Several key behaviors are observed by looking at the field data:

1. A dip in the monitoring well pressure response is observed before the pressure in the monitoring well increases.
2. The slope of the pressure change stays constant for a period of time after the dip.
3. The pressure change plateaus after increasing for some time.

These key behaviors can be analyzed using the model presented in this work.

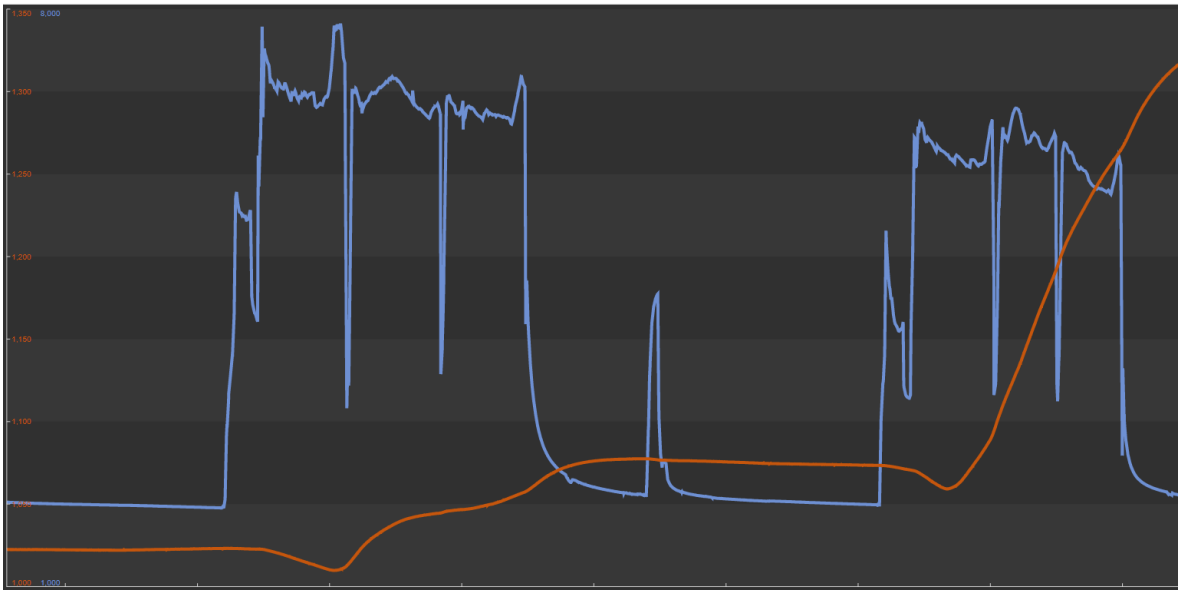

Figure 43: Field data set of treating pressure (blue) and offset gauge responses (orange). Note tensile dip before pressure in monitor well increases.

The dip in the monitor well pressure observed in the field data is caused by the tensile region ahead of an approaching fracture. The 2-D model depicts this tensile region ahead of a propagating fracture as shown in Figure 6 and Figure 21. Figure 20 (right) shows the tensile region above a fracture using the 3-D model developed in this work. These models can be used to predict the dip in the pressure induced by approaching fractures. Figure 44 shows the pressure change

induced by a finite height fracture as a function of the vertical well spacing at different locations along a monitor well. The curves are for different distances of the pressure gauge from the location where the fracture intersects the monitor wellbore. A dip in the pressure is observed when the monitoring well location is above the upper boundary of the modeled fracture.

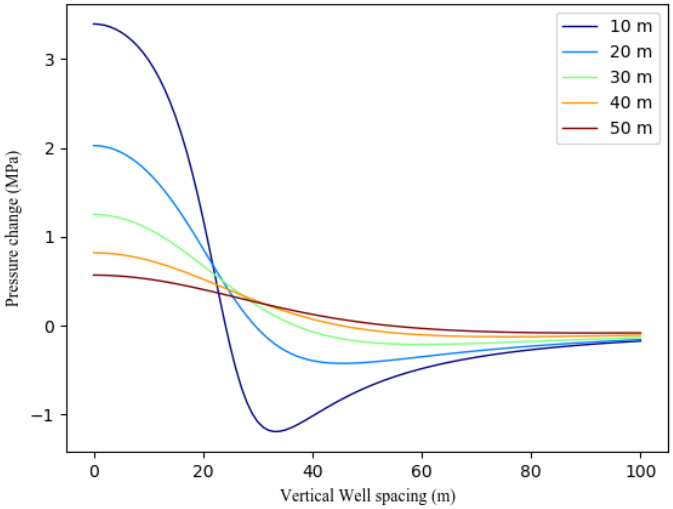

Figure 44: Pressure change observed in monitor well gauges located 10m to 50 m vertically above the plane of the well being fractured. Fracture half-length is 250m, fracture height is 50m and horizontal well spacing is 200m.

Figure 45 and Figure 46 show the impact of fracture half-length and fracture height on the pressure change observed in the monitor well gauges. Both figures show that during the initial growth of the fracture, a steep increase in the pressure change is observed, and as the fracture becomes larger, the slope gradually decreases and starts to plateau. These trends transition gradually, which is unlike what is observed in the field data. This suggests that the fractures grow in size until the plateau in the observed pressure slope is observed. The slope change in this scenario is suggestive of a fracture that has stopped growing. This could have happened because of operational changes in the treatment well, asymmetric growth of the fracture, or the growth of another fracture in the stage.

This analysis shows that using models such as the ones developed in this work can provide insight in real time to help in constraining the estimates of a propagating fracture's dimensions.

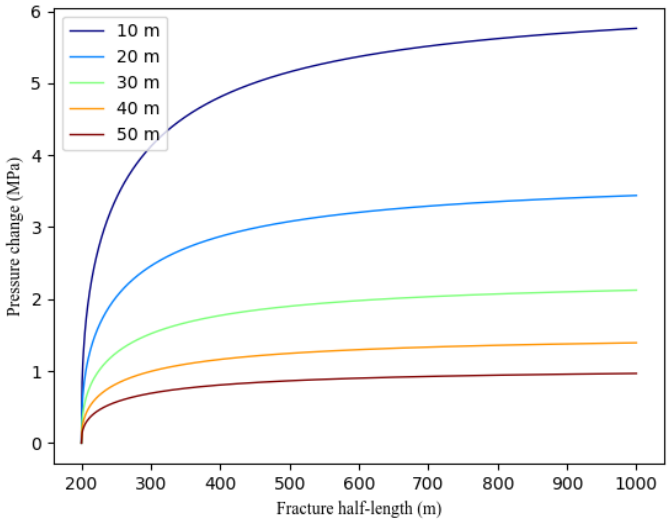

Figure 45: Pressure change observed in monitor well gauges versus fracture half length. Fracture height is 50m, horizontal well spacing is 200m and vertical well spacing is 0 m.

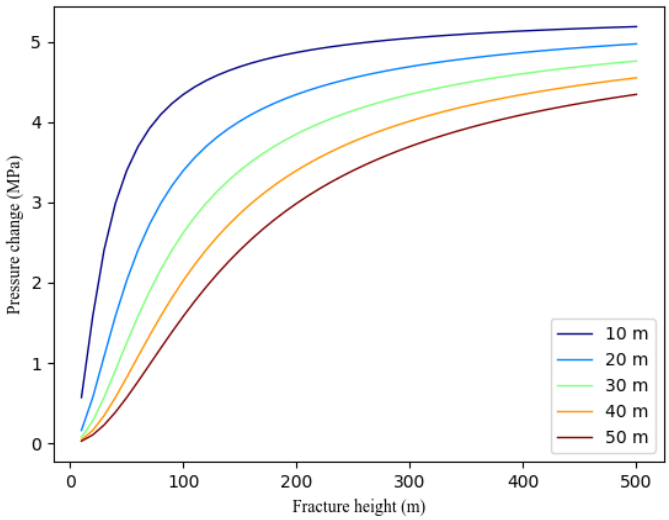

Figure 46: Pressure change observed in monitor well gauges versus fracture height. Fracture half-length is 250m, horizontal well spacing is 200 m and vertical well spacing is 0 m.

It is critical to emphasize that the slopes observed in Figure 45 and Figure 46 are for curves of pressure change versus fracture half-length and fracture height, respectively. In practice, field data is plotted versus time to see the changes in monitoring well pressure. A direct comparison of the two plots requires an estimate of length or height growth of the fractures as a function of time.

There are several models that exist to perform these calculations (Detournay 2004; Nordgren 1972; Perkins and Kern 1961). These dynamic models are beyond the scope of this work and are not needed to perform real time inversion matching from pressure data.

The presented model assumes a pressure distribution in the fracture that conforms to a constant height PKN-type fracture (Nordgren 1972). This distribution is contained in $\phi\left(\frac{x}{X_f}\right)$ in equation (8). This part of the model can easily be replaced by a pressure distribution in the fracture that is more representative of the fracture geometry. As such, the requirement of a constant height of the fracture can be removed and the model can be extended to fractures of variable height.

7.1 MULTI GAUGE FIELD CASE DESCRIPTION

The model presented in this body of work is applied to an actual field case study that consisted of multiple horizontal wells, with one being stimulated while the other had multiple bottom hole pressure gauges in the lateral. This field is known to be a strike-slip faulting regime, with fairly large horizontal stress anisotropy, which would generally yield fairly planar fracture features. The maximum stress azimuth in this area is known to be 85 degrees from north and will be used in the geometry calculations.

Contrary to many published works on fracture to fracture responses (Dawson, 2015; Seth, 2018) it is critical to compare to field cases with a higher level of certainty in the solution space for the early development of this workflow. This can be accomplished with bottom-hole pressure gauges installed in the wellbore for monitoring subsurface pressure changes. Bottom-hole pressure gauges in the well are externally ported to the formation with no pressure communication to the inside of the casing in the monitor well. Furthermore, there is no monitor fracture in these monitor wells. Pressure is being recorded at the surface during offset stimulations, and the response is a proxy for a single known point in the reservoir domain. This allows a direct comparison leading to a more refined estimate of the stress distribution and pressure around the fracture in the reservoir. An example of these externally ported gauges can be seen in Figure 47.

Figure 47: Example of Externally ported Downhole Pressure Gauges on Casing. Source: SageRider: https://www.sageriderinc.com/products/sagewatch-casing-conveyed-real-time-gauge-system)

Figure 48 describes the field case and wellbore geometries used in this study. The fracturing well to the west has a stimulation stage, which is 554 ft north and 818 ft west of the heel monitor gauge. This equates to a perpendicular distance of ~435 ft using a fracture azimuth of 85 degrees. It is important to note that an error in fracture azimuth of +/- 3 degrees can yield an error in the perpendicular distance estimate up to 40 ft, which will begin to impact the magnitude of expected poroelastic response considering the resolution of this measurement is one to tens of pounds per square inch. For this case, multiple field measurements, image logs, wellbore stability models, and microseismic data were used to develop the estimate, along with published literature examples of stress azimuth in the area, as cited by Lund Snee and Zoback (2016).

The stage pump time for this field case was 76 minutes, pumped at a rate of 90 bpm. The inflection in pressure response began to occur at 8 minutes into the pump schedule for the heel gauge and at 24 minutes for the mid-lateral gauge.

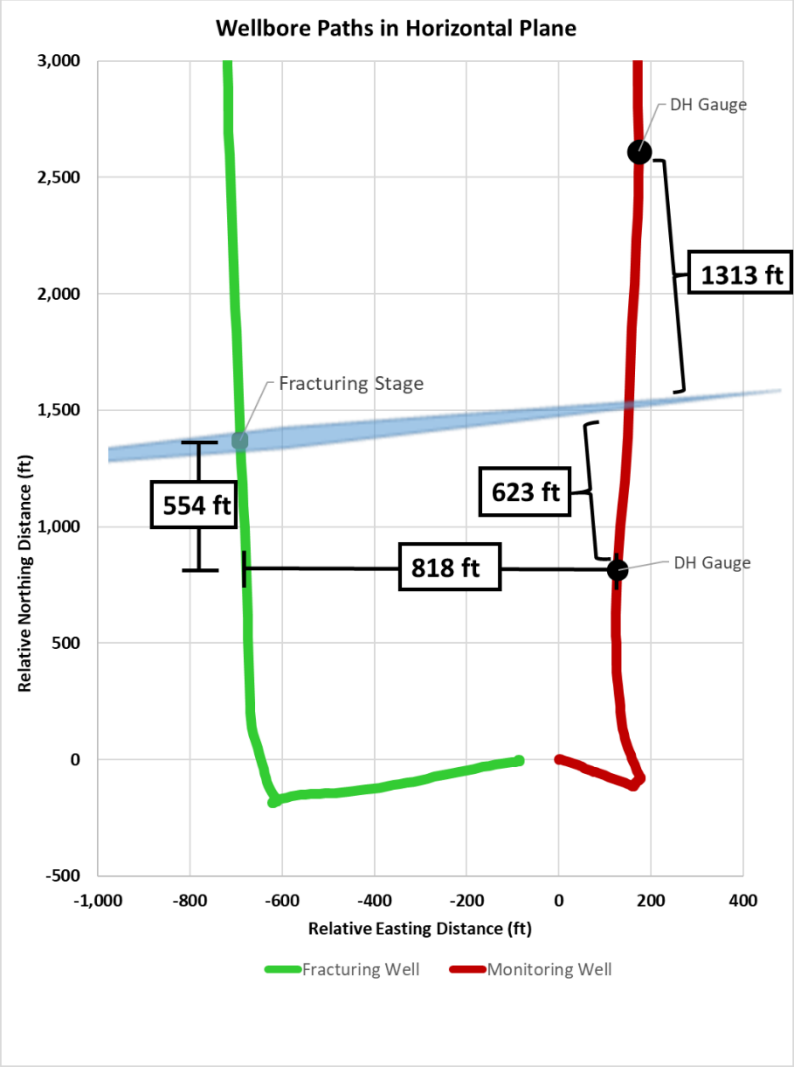

Figure 48: Horizontal wellbore trajectories and detail on stage and monitor gauge geometry

7.2 PRESSURE READINGS FROM FIELD CASE

During the stimulation of the above case in Figure 48, pressure responses were observed in the downhole gauges in the monitoring well. These pressure response trends can be seen with time in Figure 49, which show the characteristic elastic pressure response due to the fracture shadow. The interpretation for this case is that the positive inflection occurs when the propagating fracture is close and passes the downhole pressure gauge. Due to the fracture azimuth and wellbore geometry, as expected, we observe the fracture passing the monitor gauge at the heel before we

observe the response in the mid-lateral gauge. This is further explained in Appendix A, where perpendicular distances are calculated and used in the modeling comparisons.

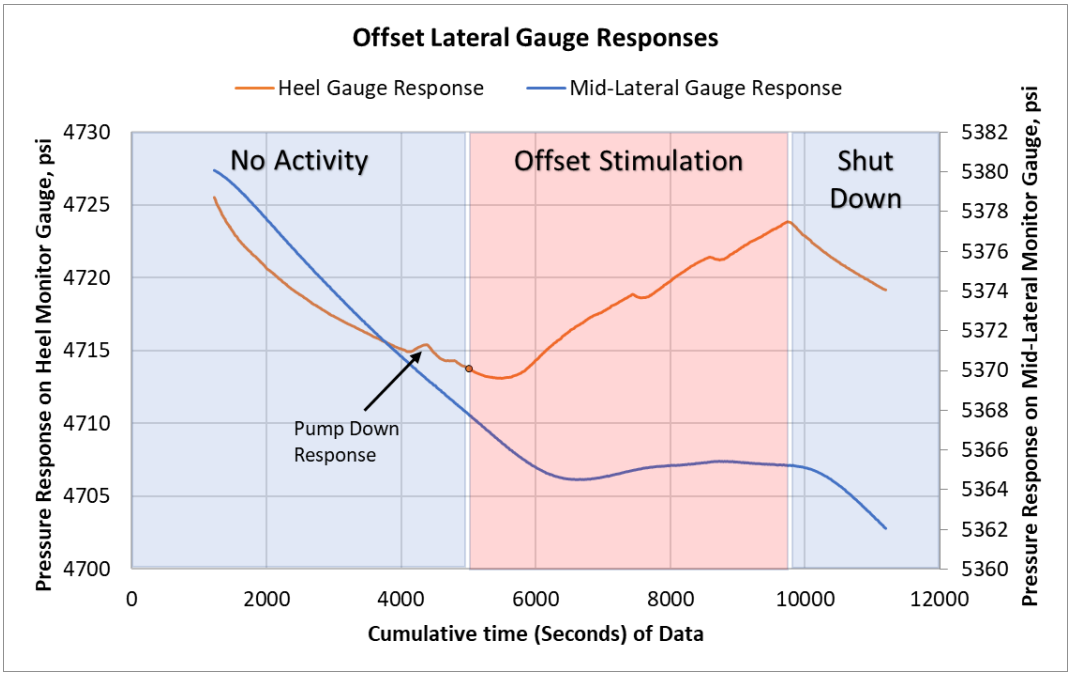

Figure 49: Offset lateral gauge responses during stimulation

To develop accurate estimates of volumetric stress increase, a critical component is to account for the leak off pressure reduction in the system must be accounted for and extrapolated to correct for true observed pressure increase at the gauge. Daneshy (2014) has provided a useful model to systematically predict such an occurrence and match the pressure falloff behavior. Utilizing this method and predicting a true pressure increase using a falloff pressure extrapolation, we can resolve a maximum pressure increase of 26.8 psi on the heel and 11.2 psi on the mid-lateral gauge.

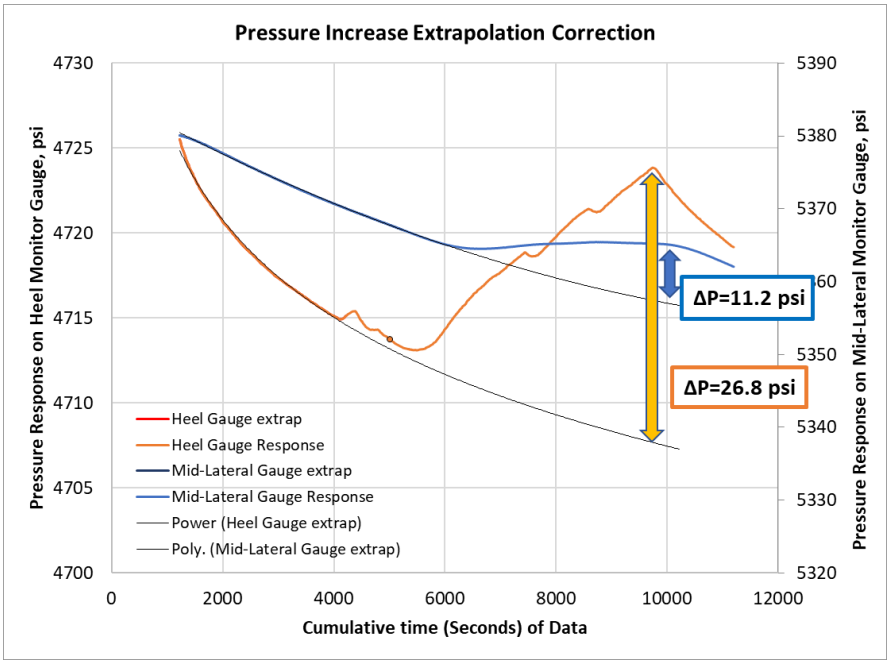

Figure 50: Pressure Extrapolation Correction for Monitoring Gauges

When investigating the magnitude of the observed pressure responses, there is a reduction in measured pressure increase with an increase in the distance from the two monitoring gauges. The heel gauge measures an overall 26.8 psi (184 kPa) response at 623 ft (190 m), and the mid-lateral gauge measures a 11.2 psi (77.2 kPa) response at 1,313 ft (400 m). A third measurement took place in an offset vertical well that was approximately 1,575 ft away from the gauge and recorded a pressure increase of 2 psi.

7.3 FIELD INVERSION WITH MULTIPLE GAUGES

For a single gauge response, one can observe the predicted volumetric stress solutions in the form of a surface which satisfies the three major conditions (P_{net}, length, height). It has been shown that from a single gauge pressure measurement, a surface of solutions can be generated and have an estimate for what type of geometry could have generated that response in previous chapters. By combining this prediction with comparative diagnostic technologies, such as fiber optics, microseismic, mappable proppant, offset pressure responses, and ISIP analysis, constraints can be made for one or more of the unknowns and shift the solution surface to a solution line. An example

of this solution line can be seen in **Error! Reference source not found.**, where fracture height has b een constrained to 480 ft. With additional measurement points, the surface or intersection of surface and solution lines can yield unique answers for fracture geometry from field measurements.

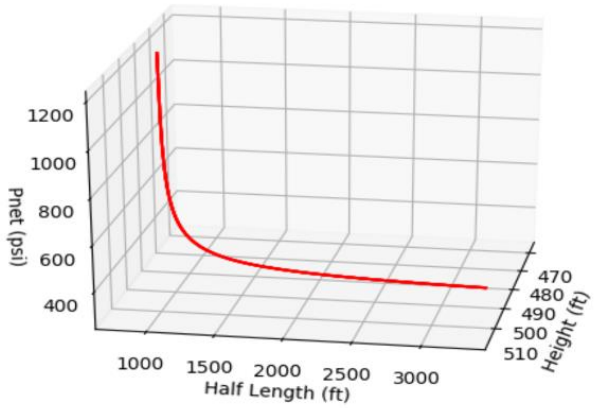

Figure 51: Geometry solution with constrained fracture height

With two downhole pressure monitoring locations, one can generate a surface solution of the two responses. This can be seen in Figure 52, which displays the most probable solution for the value of half-length and height for which the net pressure predicted by the two solutions is most similar. The colors represent the log of a minimization function, for which the minimum values (darker blue) are the most likely geometry matches. As expected with two measurements of pressure and three unknowns, this solution is only slightly constrained and hence yields a band of possible solutions. It is interesting to note there are no possible solutions below the actual lengths or distance to the gauge from the fracture tip, which provides a lower constraint on frac length. We can further constrain this solution space by including an estimate of net pressure from the ISIP of the fracturing stage.

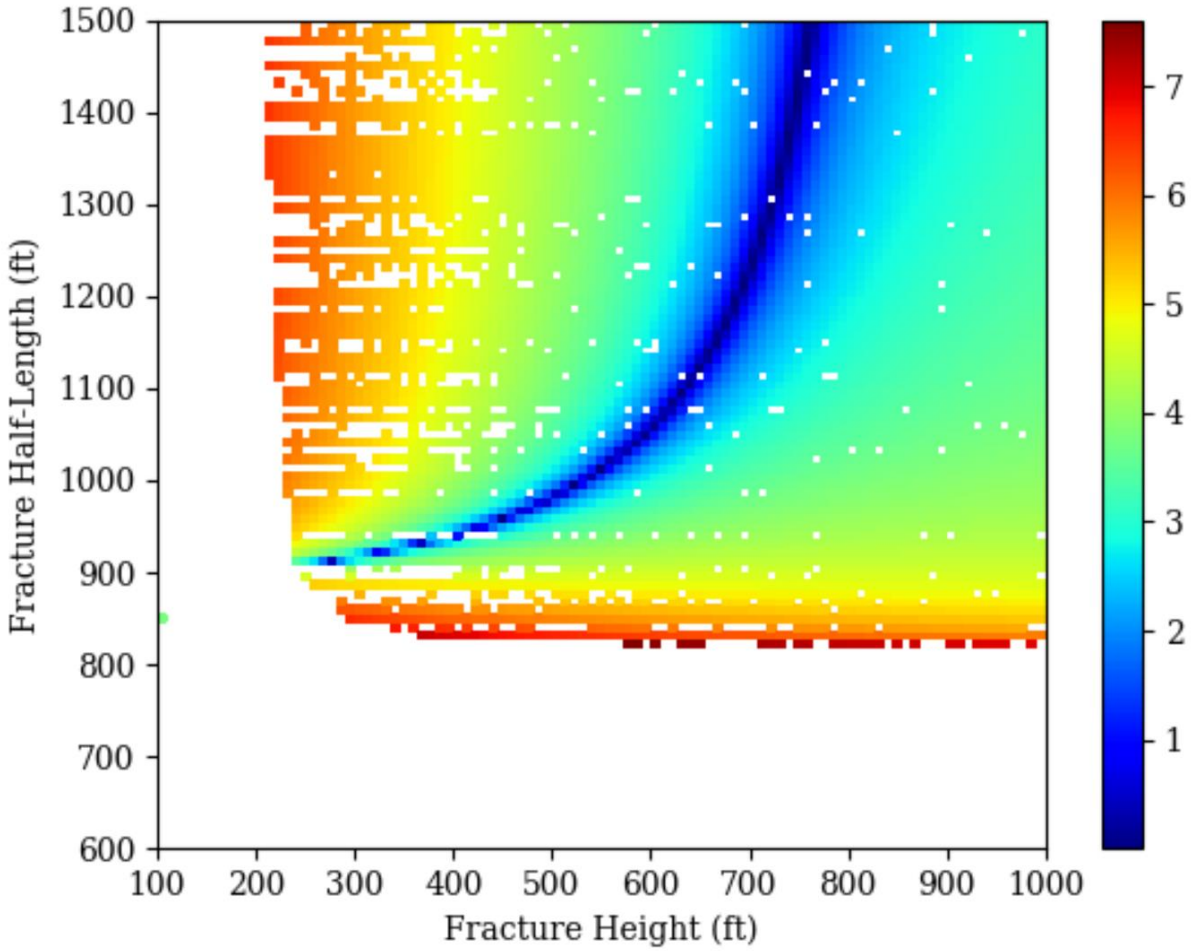

Figure 52: Most probable solution for the value of half-length and height for which the net pressure predicted by the two solutions is most similar. Blue (lower values) are possible solutions for fracture geometry.

7.4 FURTHER CONSTRAINTS IN WORKFLOW USING NET PRESSURE

An initial ISIP of 2,636 psi was observed for stage 1 of the well, and the stage ISIP for the case study calculates to be 3,400 psi, with the initial estimates of minimum horizontal stress as 5,400 psi. There was an apparent stress shadow due to sequential fracturing. A stress escalation model has been presented (Roussel, 2017) which can help estimate the incremental stress expected from inter- and intra-stage shadowing. From stage 1 to the subject stage, we observed an increase of 764 psi, which we can add to the initial S_{hmin} to yield 6,164 psi. Incorporating hydrostatic pressure for the wellbore, we can estimate a net pressure of 1,254 psi. This region of net pressure

is highlighted in Figure 53 to show the most likely regions of fracture geometry when we constrain estimates of net pressure. These results indicate a fracture height of 300 to 350 ft and a fracture half-length of 900 to 950 ft for this field case study.

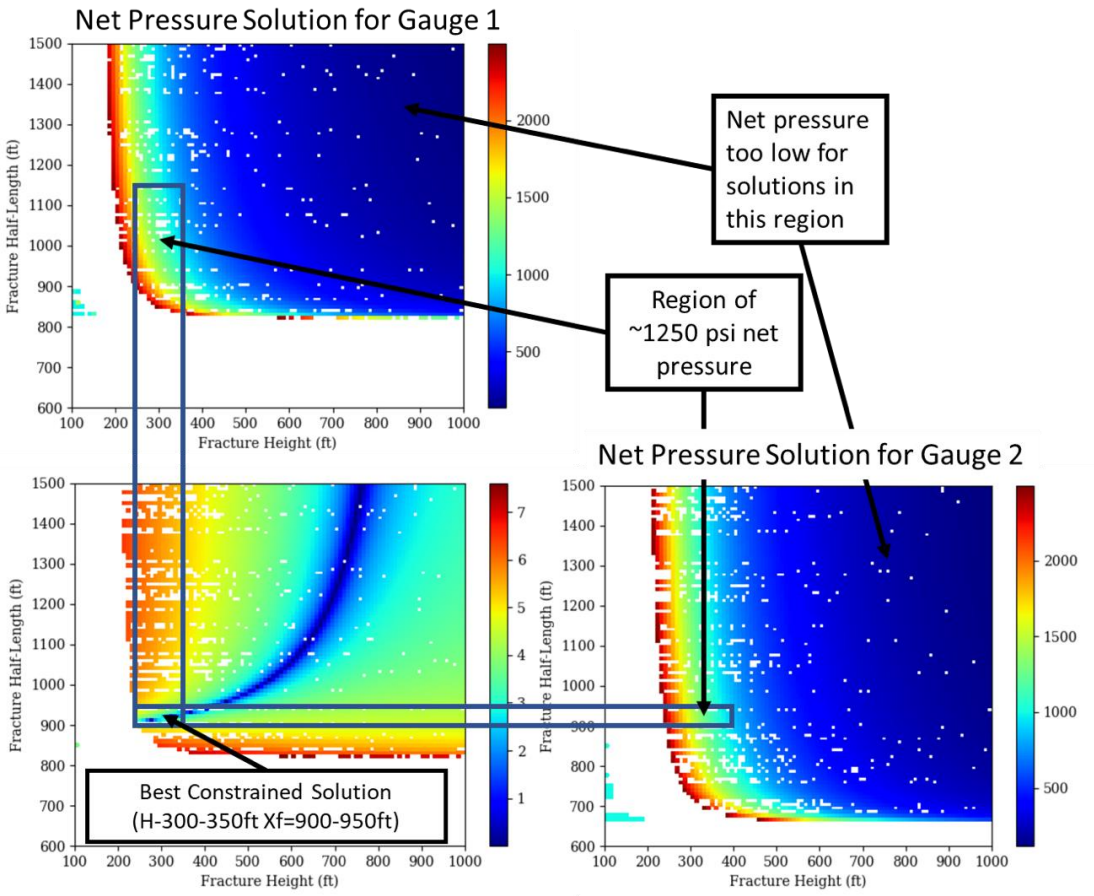

Figure 53: 2-D Surface solution using data from two pressure monitoring locations.

Chapter 8. Conclusions and Future Work

This body of work displayed the framework for a real time effort in fracture modeling. This work presents a new analytical model that provides a method for quick analysis of the fracture responses from downhole pressure gauges during treatment, validates it with fully 3-D coupled numerical modeling, and successfully applied to field cases. Multiple field stages with offset pressure responses were captured with bottom-hole gauges, interpreted, and detailed, leading to estimates of fracture geometry (height and length) in this work. When the solutions are compared to numerical results error is less than 2% for realistic viewing ranges.

Capturing live gauge data in the field and utilizing it to process and interpret fracture growth in real time (in this author's opinion) will be commonplace in the next 5-10 years. Developing the first principles reinforced workflows is crucial to utilize this technology in the future.

Future work entails continuing to advance the analytical inversion solution, and extend the model to more common field cases, such as fracture to fracture, and multi-fractures to multi-fractures. Significant additional optimization methods will need to be employed to adapt these solutions to a real time modeling effort due to the numerous potential combinations of fracture size, cluster efficiency, and complex growth. The fracture to gauge solution displayed in this work will be included in a graphical user interface to make utilization of this tool ready for the industry.

References

Ajani, A. A., & Kelkar, M. G. (2012, January 1). Interference Study in Shale Plays. Society of Petroleum Engineers. doi:10.2118/151045-MS

Awada, A., Santo, M., Lougheed, D., Xu, D., & Virues, C. (2016, October 1). Is That Interference? A Work Flow for Identifying and Analyzing Communication Through Hydraulic Fractures in a Multiwell Pad. Society of Petroleum Engineers. doi:10.2118/178509-PA

Barree, R. D., Miskimins, J. L., & Svatek, K. J. (2017, January 24). Reservoir and Completion Considerations for the Refracturing of Horizontal Wells. Society of Petroleum Engineers. doi:10.2118/184837-MS

Daneshy, A. A., Au-yeung Jessica, Thompson, T., & Tymko, D. W. (2012, January 1). Fracture Shadowing: A Direct Method for Determination of the Reach and Propagation Pattern of Hydraulic Fractures in Horizontal Wells. Society of Petroleum Engineers. doi:10.2118/151980-MS

Daneshy, A. A., & Pomeroy, M. D. (2012, January 1). In-situ Measurement of Fracturing Parameters from Communication Between Horizontal Wells. Society of Petroleum Engineers. doi:10.2118/160480-MS

Daneshy, Ali. 2017. "Analysis of Front and Tail Stress Shadowing in Horizontal Well Fracturing: Their Consequences With Case History." in *SPE Hydraulic Fracturing Technology Conference and Exhibition*. Society of Petroleum Engineers.

Daneshy, A. A. (2014, October 27). Fracture Shadowing: Theory, Applications and Implications. Society of Petroleum Engineers. doi:10.2118/170611-MS

Dawson, M., & Kampfer, G. (2016, August 1). Breakthrough in Hydraulic Fracture & Proppant Mapping: Achieving Increased Precision with Lower Cost. Unconventional Resources Technology Conference. doi:10.15530/URTEC-2016-2432330

Detournay, E. 2004. "Propagation Regimes of Fluid-Driven Fractures in Impermeable Rocks." *International Journal of Geomechanics* 4(1):35–45.

Elliott, B. 2018 source data written up for the SPE fracture driven communication report, unpublished

Elliott, B., Manchanda, R., Seth, P., & Sharma, M. (2019, July 31). Interpreting Inter-Well Poroelastic Pressure Transient Data: An Analytical Approach Validated with Field Case Studies. Unconventional Resources Technology Conference. doi:10.15530/urtec-2019-449

Elliott, Brendan. "19HFTC Plenary Session Presentations." *SPE Digital Assets: Collection Preview*, Society of Petroleum Engineeers, 5 Feb. 2019, spe.widencollective.com/c/yjgm9v1w.

Gala, D. P., Manchanda, R., & Sharma, M. M. (2018, August 9). Modeling of Fluid Injection in Depleted Parent Wells to Minimize Damage Due to Frac-Hits. Unconventional Resources Technology Conference. doi:10.15530/URTEC-2018-2881265

Green, A. E. and I. N. Sneddon. 1950. "The Distribution of Stress in the Neighbourhood of a Flat Elliptical Crack in an Elastic Solid." *Mathematical Proceedings of the Cambridge Philosophical Society* 46(01):159.

Haustveit, K., Dahlgren, K., Greenwood, H., Peryam, T., Kennedy, B., & Dawson, M. (2017, January 24). New Age Fracture Mapping Diagnostic Tools-A STACK Case Study. Society of Petroleum Engineers. doi:10.2118/184862-MS

Hwang, J., Szabian, M. J., & Sharma, M. (2017, July 24). Hydraulic Fracture Diagnostics and Stress Interference Analysis by Water Hammer Signatures in Multi-Stage Pumping Data. Unconventional Resources Technology Conference. doi:10.15530/URTEC-2017-2687423

Jones E, Oliphant E, Peterson P, et al. SciPy: Open Source Scientific Tools for Python, 2001, http://www.scipy.org/ [Online; accessed 2019-04-26

Kampfer, Günther, D. Ph, Statoil Asa, Matthew Dawson, and D. Ph. 2016. "A Novel Approach to Mapping Hydraulic Fractures Using Poromechanic Principles." *ARMA*.

King, G. E., Rainbolt, M. F., & Swanson, C. (2017, October 9). Frac Hit Induced Production Losses: Evaluating Root Causes, Damage Location, Possible Prevention Methods and Success of Remedial Treatments. Society of Petroleum Engineers. doi:10.2118/187192-MS

Kurtoglu, B., & Salman, A. (2015, November 9). How to Utilize Hydraulic Fracture Interference to Improve Unconventional Development. Society of Petroleum Engineers. doi:10.2118/177953-MS

Lawal, H., Jackson, G., Abolo, N., & Flores, C. (2013, June 10). A Novel Approach To Modeling and Forecasting Frac Hits In Shale Gas Wells. Society of Petroleum Engineers. doi:10.2118/164898-MS

Lawal, H., Abolo, N., Jackson, G., Sahai, V., & Flores, C. P. (2014, May 21). A Quantitative Approach to Analyze Fracture Area Loss in Shale Gas Reservoirs. Society of Petroleum Engineers. doi:10.2118/169406-MS

Lehmann, J., Budge, J., Palghat, A., Petr, C., & Pyecroft, J. (2016, February 1). Expanding Interpretation of Interwell Connectivity and Reservoir Complexity through Pressure Hit Analysis and Microseismic Integration. Society of Petroleum Engineers. doi:10.2118/179173-MS

Lindsay, G., Miller, G., Xu, T., Shan, D., & Baihly, J. (2018, January 23). Production Performance of Infill Horizontal Wells vs. Pre-Existing Wells in the Major US Unconventional Basins. Society of Petroleum Engineers. doi:10.2118/189875-MS

Lund Snee, Jens-Erik & D. Zoback, Mark. (2016). State of stress in Texas: Implications for induced seismicity. Geophysical Research Letters. 43. 10.1002/2016GL070974.

Mack, M. G., Taylor, S. M., Rich, J., Kahn, D., King, J., Schaeffer, B., … Biholar, A. (2017, August 7). Can Moment Tensor Inversion Aid Engineering Decisions? A Delaware Basin Case Study. Unconventional Resources Technology Conference. doi:10.15530/URTEC-2017-2693686

Manchanda, Ripudaman. 2015. "A General Poro-Elastic Model for Pad-Scale Fracturing of Horizontal Wells."

Manchanda, Ripudaman, Shuang Zheng, Sho Hirose, and Mukul M. Sharma. 2019. "Integrating Reservoir Geomechanics with Multiple Fracture Propagation and Proppant Placement." SPE Journal under review

Manchanda, Ripudaman, Elliott, B., Seth, P. and Sharma, M.M. (2019) Interpreting Inter-Well Poroelastic Pressure Transient Data: An Analytical Approach. accepted.

Manchanda, R., Bhardwaj, P., Hwang, J., & Sharma, M. M. (2018, January 23). Parent-Child Fracture Interference: Explanation and Mitigation of Child Well Underperformance. Society of Petroleum Engineers. doi:10.2118/189849-MS

Martinez, R., Rosinski, J., & Dreher, D. T. (2012, January 1). Horizontal Pressure Sink Mitigation Completion Design: A Case Study in the Haynesville Shale. Society of Petroleum Engineers. doi:10.2118/159089-MS

Miller, G., Lindsay, G., Baihly, J., & Xu, T. (2016, May 5). Parent Well Refracturing: Economic Safety Nets in an Uneconomic Market. Society of Petroleum Engineers. doi:10.2118/180200-MS

Morales, A., Zhang, K., Gakhar, K., Marongiu Porcu, M., Lee, D., Shan, D., … Acock, A. (2016, February 1). Advanced Modeling of Interwell Fracturing Interference: An Eagle Ford Shale Oil Study - Refracturing. Society of Petroleum Engineers. doi:10.2118/179177-MS

Nordgren, R. P. 1972. "Propagation of a Vertical Hydraulic Fracture." *Society of Petroleum Engineers Journal* 12(04):306–14.

Perkins, T. K. and L. R. Kern. 1961. "Widths of Hydraulic Fractures." *Journal of Petroleum Technology* 13(09):937–49.

Roussel, N. P. (2017, January 24). Analyzing ISIP Stage-by-Stage Escalation to Determine Fracture Height and Horizontal-Stress Anisotropy. Society of Petroleum Engineers. doi:10.2118/184865-MS

Roussel, N. P., & Agrawal, S. (2017, July 24). Introduction to Poroelastic Response Monitoring - Quantifying Hydraulic Fracture Geometry and SRV Permeability from Offset-Well

Pressure Data. Unconventional Resources Technology Conference. doi:10.15530/URTEC-2017-2645414

Rainbolt, M. F., & Esco, J. (2018, January 23). Frac Hit Induced Production Losses: Evaluating Root Causes, Damage Location, Possible Prevention Methods and Success of Remediation Treatments, Part II. Society of Petroleum Engineers. doi:10.2118/189853-MS

Seth, Puneet, Ripudaman Manchanda, Ashish Kumar, and Mukul Sharma. 2018. "Estimating Hydraulic Fracture Geometry by Analyzing the Pressure Interference Between Fractured Horizontal Wells." in *SPE Annual Technical Conference and Exhibition*. Society of Petroleum Engineers.

Seth, Puneet, Ripudaman Manchanda, Shuang Zheng, Deepen Gala, and Mukul Sharma. 2019. "Poroelastic Pressure Transient Analysis: A New Method for Interpretation of Pressure Communication Between Wells During Hydraulic Fracturing." In SPE Hydraulic Fracturing Technology Conference and Exhibition. Society of Petroleum Engineers. https://doi.org/10.2118/194358-MS.

Seth, P., Shrivastava, K., Kumar, A. and Sharma M.M. 2019. Pressure Interference between Fractured Horizontal Wells: Impact of Complex Fracture Growth on Offset Well Pressure Measurements. Accepted for publication at the 53rd US Rock Mechanics/Geomechanics Symposium to be held in New York, NY, USA, 23–26 June 2019.

Seth, P., Manchanda, R., Elliott, B., Zheng, S. and Sharma M.M. 2019. Diagnosing Multi-Cluster Fracture Propagation Using Dynamic Poroelastic Pressure Transient Analysis. Accepted for publication at the Unconventional Resources Technology Conference to be held in Denver, Colorado, USA, 22-24 July 2019.

Seth, P., Manchanda, R., Elliott, B., Zheng, S. and Sharma M.M. 2019. Estimating Fracture Network Area and SRV Permeability by Analyzing Offset Well Pressure Measurements during Fracturing. Accepted for publication at the SPE Annual Technical Conference and Exhibition to be held in Calgary, Alberta, Canada, 30 September - 2 October 2019.

Sneddon, I. N., The distribution of stress in the neighbourhood of a crack in an elastic solid187Proceedings of the Royal Society of London. Series A. Mathematical and Physical Sciences. http://doi.org/10.1098/rspa.1946.0077

Spicer, S., & Coenen, E. (2018, August 9). Estimation of Fracture Geometries From Poroelastic Pressure Responses in Offset Wells. Unconventional Resources Technology Conference. doi:10.15530/URTEC-2018-2886118

Warpinski, N. R., S. L. Wolhart, and C. a. Wright. 2004. "Analysis and Prediction of Microseismicity Induced by Hydraulic Fracturing." SPE Journal 9(01):24–33.

Yu, W., Xu, Y., Weijermars, R., Wu, K., & Sepehrnoori, K. (2017, January 24). Impact of Well Interference on Shale Oil Production Performance: A Numerical Model for Analyzing Pressure Response of Fracture Hits with Complex Geometries. Society of Petroleum Engineers. doi:10.2118/184825-MS

Zhe, L., Younis, R., & Jiang, J. (2016, August 1). A Diagnostic Framework for Bashed; Wells in Unconventional Reservoirs: A Numerical Simulation and Model Selection Theory Approach. Unconventional Resources Technology Conference. doi:10.15530/URTEC-2016-2448463

Zheng, S., Manchanda, R., Sharma, M.M., 2019. Development of a fully implicit 3-D geomechanical fracture simulator. J. Pet. Sci. Eng. 179, 758–775. https://doi.org/10.1016/j.petrol.2019.04.065

Vita

Brendan Elliott is a senior staff completions engineer at Devon Energy working in a corporate subsurface technology role. His main responsibilities include completion design and optimization, DFIT analysis, fracture diagnostics and complex multi-interval planning. Currently focused in the Delaware Basin, developing multiple stacked pay intervals and leads a subsurface technical team to investigate depletion mitigation and fracture interference. Brendan holds a BS in Petroleum Engineering From Texas A&M University, and is pursuing his MS & PhD at the University of Texas while working remotely for Devon.

Permanent contact email <Brendan07elliott@gmail.com>